American Journal of Mechanical Engineering, 2017, Vol. 5, No. 5, 175-198
Available online at http://pubs.sciepub.com/ajme/5/5/1

DOI:10.12691/ajme-5-5-1

Graphite-Epoxy Composite Design for Aircraft Wing Skin Using Computational Techniques - Part II

Akindapo Jacob Olaitan*, Johnson-Anamemena Nnaemeka, Garba Danladi King

Department of Mechanical Engineering, Nigerian Defence Academy, Kaduna, Nigeria
*Corresponding author: jacobakindapo@gmail.com

Abstract This present work is on graphite-epoxy design for light weight high performance structure of an aircraft wing skin using computational technique. MATLAB MuPAD software was used to derive an analytical model for aircraft wing loads using symbolic computation to estimate the shear force acting on the wings while Autodesk Simulation Composite Design and ANSYS 14 Mechanical APDL (ANSYS Parametric Design Language) software were used to design and analyze the idealized composite structures of the wing skin. An idealized structure such as a flat plate which is a good approximation for the purposes of preliminary design and analysis was first developed using Autodesk Simulation Composite Design. After which, finite element analysis was also employed using ANSYS 14 Mechanical APDL to provide progressive failure analyses of the graphite-epoxy composite structures in order to determine the in-plane shear stress, displacement and other desired mechanical properties that would aid in material selection during fabrication and manufacturing. This investigation reveals that to withstand shear force of 3,000N for wing skin laminates designs, High Modulus (HM) and Ultra Modulus (UM) with [(+/-45)s] stacking sequence offers the best maximum shear stress output of 0.199×10^{10} N/m^2 prior to delamination. For failure prediction, Low Modulus (LM) and Ultra Modulus (UM) with [(+/-45)s] design has the best property prior to failure at 0.499×10^{10} N/m^2. HM and UM with [(+/-45/0/90)s] stacking sequence demonstrates the least compressive deformation of 0.004195m.

Keywords: *aircraft wing skin, epoxy, graphite, high modulus, low modulus, ultra modulus*

Cite This Article: Akindapo Jacob Olaitan, Johnson-Anamemena Nnaemeka, and Garba Danladi King, "Graphite-Epoxy Composite Design for Aircraft Wing Skin Using Computational Techniques - Part II." *American Journal of Mechanical Engineering*, vol. 5, no. 5 (2017): 175-198. doi: 10.12691/ajme-5-5-1.

1. Introduction

The importance of composite materials is far reaching as it is not only used in the aerospace industry, but also in a large and increasing number of commercial mechanical applications, such as internal combustion engines, machine components, thermal control and electronic packaging, automobile, train and aircraft structures and mechanical components, such as brakes, drive shafts, flywheels, tanks, and pressure vessels, dimensionally stable components, process industries equipment requiring resistance to high-temperature corrosion, oxidation and wear, offshore and onshore oil exploration and production equipment, marine structures; sports and leisure equipment, including biomedical devices.

William and David in 2010 described composite materials as materials with two phases; one is termed the matrix, which is continuous and surrounds the other phase, often called the dispersed phase. The properties of composites are functions of the properties of the constituent phases, their relative amounts, and the geometry of the dispersed phase. Dispersed phase geometry in this context means the shape of the particles and the particle size, distribution, and orientation [15].

Generally, composites tend to have the following characteristics; high strength, high modulus, low density, excellent resistance to fatigue, creep, creep rupture, corrosion, wear and low coefficient of thermal expansion [5].

For applications in which both mechanical properties and low weight are important, useful attributes are specific strength and specific stiffness. In this work, composite material is being designed for use in the construction of small passenger aircraft wings with Airbus A380 as a case study.

The European Aircraft Company, Airbus, in an attempt to meet up with the demand for air travels which have increased tremendously by an average of 4.6% [9], developed a bigger plane and higher capacity (Airbus A380 the world's largest passenger airliner) which can carry a total of 853 passengers in a single-class economy configuration with maximum weight of 50,000 kilogram [1]. Under extreme conditions particularly during take-off and landing enormous forces act on the wing which may distort the tips of the wing upwards by more than 7 meters with the total length of the wing from tip to fuselage being 36.3 meters (wingspan 79.75 meters) in comparison to the smallest wing on its fleet, that of A318-A321 which is 14.5 meters (wingspan 34.9 meters) [4]. It used to be that aircraft on this scale could only handle these forces by using special steels or aluminium alloys, but always at the expense of weight.

Unlike steel or aluminium, textile fiber materials often referred to as technical fibers can save weight simply by

determining the direction of the acting external forces. The stability of the materials can be affected by placing the stability providing fibers appropriate to the direction of the external forces that are acting on the structural part. For example, for parts stressed by torsion would be at 45^0 to the length of the component. The basic material is carbon/graphite fiber.

Airbus over the years has constantly increased its use of composite materials for their attendant benefits in the areas of manufacturing, design and use. In manufacturing, lower production costs, quality robustness and reduction of lead time have been experienced. There have been great design improvements and reduced lifecycle costs for trade-offs with composites [1].

2. Review of Existing Literatures

Shabeer and Murtaza in 2013 developed an accurate model for optimal design through designing the structure of a wing that combined composite (skin) and isotropic materials, and then compared it with a similar wing made by changing the orientation of composite ply in the skin. The optimum design was obtained by comparing stress and displacements. Structural modeling was completed with the help of CATIA V5 after which finite element modeling was performed using MSc Patran. The optimum design showed that the largest magnitude of displacement was obtained at the free end of the combined wing, the replacement of aluminium alloy by graphite/epoxy reduces the total weight of the aircraft wing by 23.7%, and displacement corresponding to the ply sequence [0/90/+ 45/-45/90/0] is of value 4.63mm and the von Mises stress corresponding to this sequence is $49.8N/mm^2$. By comparing the stresses and displacements of the various designs used they concluded that the ply sequence [0/90/+45/-45/90/0] is seen to have better performance. Thus, they opined that it is desirable to adopt the ply sequence [0/90/+45/-45/90/0] for composite aircraft wings in comparison with the other ply sequences considered in their study [11].

Sudhir and Sujatha in 2015 designed and analyzed a general aviation airplane wing. The design process started with a sketch of how the airplane is envisioned. Weight was estimated based on the sketch and a chosen design mission profile. A more refined method was conducted based on calculated performance parameters to achieve a more accurate weight estimate which was used to acquire the external geometry of the airplane. A three-dimensional layout of the airplane was created using RDS software based on conic lifting, then placed in a simulation environment in Matlab which proved the designs adherence to the design goals. In addition, static stress analysis was also performed for wing design purposes. Using the finite element software package COMSOL, the calculated aerodynamic loads were applied to the wing to check the wing reliability. It was shown that the designed wing could be a good candidate for similar general aviation airplane implementation. The aircraft wing model was created by CATIA V5 R20 software. Then, the model created by CATIA was imported to ANSYS 14.5 software. It was observed that aircraft wing with AA7075 obtained 144MPa and 0.59mm stress level and displacement respectively while the composite material model, GLARE (glass-reinforced aluminum laminate), obtained 53.03MPa and 0.046mm respectively. By using the composite material GLARE lower deformation was observed on the aircraft wing [12].

James et al in 2010 carried out an airframe wingbox preliminary design and weight prediction where they employed the use of HyperSizer commercial software for the analysis and design of composite and metallic aircraft structures. Their study focused on trade studies performed on an aircraft wingbox structure. The wingbox is modeled after a commercial transport jet. The loads on the upper and lower wing skin surface are axially compression paired with high shear loading caused by wing twist. Weight trends were quantified considering all possible design possibilities in order to determine the most structurally efficient combination of composite layups and panel cross section dimensions to achieve the lightest weight. Results were obtained with HyperSizer for Metallic Integral Blade and Bonded Zee Stiffened panel concepts as well as Composite Hat and Tee Stiffened panel concepts. The HyperSizer optimum designs scored based on the weight maturity level (WML) of the panel design. The study showed that the composite hat stiffened panel is the lightest concept for a wingbox structure and is 30% lighter than the lightest metallic design [6].

Sidda, Suresh and Vijaya in 2013 investigated the use of D-optimal designs in the Design of Experiments (DOE) and Artificial Neural Networks (ANN) in predicting the deflection and stresses of Carbon Fiber Reinforced Plastic (CFRP) square laminated composite plate subjected to uniformly distributed load. For training and testing of the ANN model, a number of finite element analyses were carried out using D-optimal designs by varying the fiber orientations and thickness of each lamina. The composite plate was modeled using shell 99 elements of ANSYS software. The ANN model was developed using Multilayer Perceptron (MLP) back propagation algorithm. The adequacy of the developed model was verified by root mean square error and regression coefficient. The results showed that the training algorithm of back propagation was sufficient enough in predicting the deflection and stresses. The ANN predicted results were in very good agreement with the finite element results. This suggested that, the D-optimal design of experiments can be applied to any structural analysis. The D-optimal set of laminates is not limited to 10 ply laminates for changing the ply thickness. It is applicable to laminates of any number of plies by changing the ply thickness. The effectiveness of the method is shown with predicting capability to deflection and stresses of laminated composite plates subjected to uniformly distributed load under simply supported boundary condition [13].

Hassan, Wahab, Riaz and Iqbal in 2013 did a 3-D CAD modeling and analysis of aircraft wing using CATIA software and compared its result with that of ANSYS software. CAD modeling of the complete wing of a fighter aircraft was done in CATIA analysis. The model was also analyzed in ANSYS software for comparison of results. The results were compared between both software and an error of 3.88% was observed. These results were further compared with actual experimental static testing results with an error of 5%. With same computing time the results

were reasonably close in both of the software. For complex geometries, a small deviation of results was observed due to the simplifications done for the ANSYS model. Although, CATIA is not a pure FEM software, however, the results were comparable with ANSYS software for linear analysis. The distinct advantages of modeling in CATIA were found to be accuracy of model, parametric modeling, Linear FEM analysis, ease of machining, and generation of a layout model. CAD model in CATIA allowed rapid changing of design during the design stage and its preliminary linear analysis, saving both time and reducing costs considerably [14].

This work investigates the graphite-epoxy composite design for aircraft wing skin using computational techniques.

3. Analysis of Laminates

Generally laminas are stacked at various orientations to assemble a laminate.

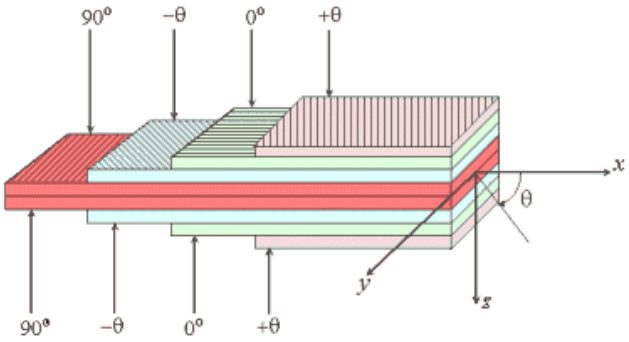

Figure 1. Laminate with stacking sequence $[\theta, 0, -\theta, 90]_s$

3.1. Governing Equations for Laminate Design

The stress-strain relationship for composite materials is not linear. However, to simplify the calculations it is assumed that for all composites, elastic modulus is constant and Hooke's law can be applied [10].

Mathematically, stress is defined as;

$$\sigma = E\varepsilon \tag{1}$$

Where the stress is σ, strain is ε and elastic modulus is E.

For Two Dimensional State of Stress (Plane Stress) for Composite Laminate;

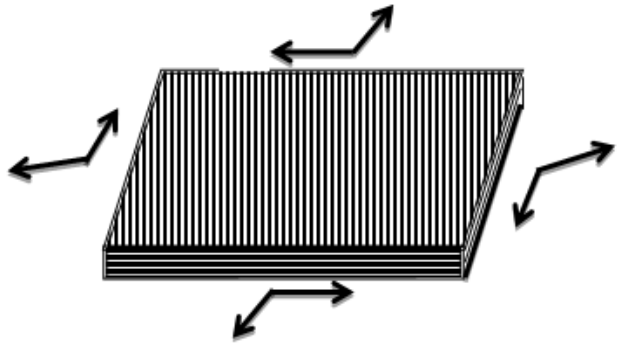

Figure 2. Two dimensional state of stress

The material sketch is defined as [10];

$$\begin{bmatrix}\sigma_1\\ \sigma_2\\ \sigma_6\end{bmatrix} = \begin{bmatrix}Q_{11} & Q_{12} & 0\\ Q_{21} & Q_{22} & 0\\ 0 & 0 & Q_{66}\end{bmatrix}\begin{bmatrix}\varepsilon_1\\ \varepsilon_2\\ \varepsilon_6\end{bmatrix} \tag{2}$$

Where the column matrix of stress is $[\sigma]$, stiffness matrix is $[Q]$ and column matrix of strain is [ε].

$$Q_{11} = \frac{E_{11}}{(1-V_{12}V_{21})} \tag{3}$$

$$Q_{22} = \frac{E_{22}}{(1-V_{12}V_{21})} \tag{4}$$

$$Q_{12} = Q_{21} = \frac{V_{21}E_{11}}{(1-V_{12}V_{21})} = \frac{V_{12}E_{22}}{(1-V_{12}V_{21})} \tag{5}$$

$$Q_{66} = G. \tag{6}$$

3.2. Determination of Plane Strain

The strain matrix can be defined as;

$$[\varepsilon] = [S][\sigma] \tag{7}$$

Where the compliance matrix is $[S]$.

3.3. Determination of the Off-axis Orthotropic Lamina Properties Using Transformation Matrix $[T]$

The stress and strain components are defined as;

$$\begin{bmatrix}\sigma_1\\ \sigma_2\\ \sigma_6\end{bmatrix} = [T]\begin{bmatrix}\sigma_x\\ \sigma_y\\ \sigma_z\end{bmatrix} \tag{8}$$

$$\begin{bmatrix}1\\ 2\\ 3/2\end{bmatrix} = [T]\begin{bmatrix}x\\ y\\ xy/2\end{bmatrix} \tag{9}$$

Where,

$$[T] = \begin{vmatrix}m^2 & n^2 & 2mn\\ n^2 & m^2 & -2mn\\ -mn & mn & m^2-n^2\end{vmatrix} \tag{10}$$

$$m = \cos\theta \text{ and } n = \sin\theta.$$

The laminate mechanical properties are determined as a function of $'\theta'$.

It is obvious from equations (2) through (10) that the stresses in the laminate can be expressed as;

$$\begin{bmatrix}\sigma_x\\ \sigma_y\\ \sigma_z\end{bmatrix} = \left[\bar{Q}\right]_k\begin{bmatrix}\varepsilon_x\\ \varepsilon_y\\ \varepsilon_{xy}\end{bmatrix} \tag{11}$$

Where,

$$\left[\bar{Q}\right]_k = \begin{vmatrix} \bar{Q}_{11} & \bar{Q}_{12} & \bar{Q}_{16} \\ \bar{Q}_{21} & \bar{Q}_{22} & \bar{Q}_{26} \\ \bar{Q}_{61} & \bar{Q}_{62} & \bar{Q}_{66} \end{vmatrix}_k . \quad (12)$$

The definitions of terms in equation (12) are;

$$\bar{Q}_{11} = Q_{11}m^4 + 2\left(Q_{12} + 2Q_{66}\right)m^2n^2 + Q_{22}n^4 \quad (13)$$

$$\bar{Q}_{22} = Q_{11}n^4 + 2\left(Q_{12} + 2Q_{66}\right)m^2n^2 + Q_{22}m^4 \quad (14)$$

$$\bar{Q}_{66} = \left(Q_{11} + Q_{22} - 2Q_{12} - 2Q_{66}\right)m^2n^2 + Q_{66}\left(m^4 + n^4\right) \quad (15)$$

$$\bar{Q}_{12} = \left(Q_{11} + Q_{22} - 4Q_{66}\right)m^2n^2 + Q_{12}\left(m^4 + n^4\right) \quad (16)$$

$$\bar{Q}_{16} = \left(Q_{11} - Q_{12} - 2Q_{66}\right)m^3n + \left(Q_{12} - Q_{22} + 2Q_{66}\right)mn^3 \quad (17)$$

$$\bar{Q}_{26} = \left(Q_{11} - Q_{12} - 2Q_{66}\right)mn^3 + \left(Q_{12} - Q_{22} + 2Q_{66}\right)m^3n \quad (18)$$

k = lamina number.

3.4. In-plane Loads for a Balanced Orthotropic Laminate

This is a laminate in which for every lamina at plus 'θ' orientation, there is a corresponding similar lamina at minus 'θ' orientation, and they are defined in N/m by [10];

$$\begin{bmatrix} N_x \\ N_y \\ N_{xy} \end{bmatrix} = \begin{vmatrix} A_{11} & A_{12} & 0 \\ A_{21} & A_{22} & 0 \\ 0 & 0 & A_{66} \end{vmatrix} \begin{bmatrix} \varepsilon_x \\ \varepsilon_y \\ \varepsilon_{xy} \end{bmatrix} \quad (19)$$

Where,

N_i = Load in the direction of i.

$$A_{ij} = \sum_{k=1}^{n} \left(\bar{Q}_{ij}\right)_k \times t_k . \quad (20)$$

3.5. Determination of Margin of Safety (M.S.) for Strains in the Various Axes

The margins of safety for strains along the various axes are defined as;

$$M.S._1 = \frac{\frac{tu}{1}}{2\times_x} - 1 \quad (21)$$

$$M.S._2 = \frac{\frac{tu}{2}}{2\times_y} - 1 \quad (22)$$

$$M.S._6 = \frac{\frac{su}{6}}{2\times_{xy}} - 1. \quad (23)$$

The applied factor of safety is 2.0 which is commonly used for composite materials and only a margin of safety greater than 0 must be demonstrated.

3.6. Governing Equations for Rule of Mixture

To find the optimum thickness 'T_1' and 'T_2' for any mixture of fabrics, the following governing equations can be used [10];

$$T_1 = \frac{2N_1 \times \sigma_{22} - 2N_2 \times \sigma_{21}}{\sigma_{11} \times \sigma_{22} - \sigma_{12} \times \sigma_{21}} \quad (24)$$

$$T_2 = \frac{2N_1 \times \sigma_{12} - 2N_2 \times \sigma_{11}}{\sigma_{21} \times \sigma_{12} - \sigma_{11} \times \sigma_{22}}. \quad (25)$$

3.7. Strain-Displacement Relations

The strain displacement relations for infinitesimal strains using the displacement field can be expressed as [8];

$$\varepsilon_{xx} = \varepsilon_{xx}^0 + zk_{xx} \quad (26)$$

$$\varepsilon_{yy} = \varepsilon_{yy}^0 + zk_{yy} \quad (27)$$

$$2\varepsilon_{xy} = 2\varepsilon_{xy}^0 + 2zk_{xy}. \quad (28)$$

Equations (26) through (28) can be expressed as;

$$\left\{\varepsilon_x\right\} = \left\{\varepsilon^0\right\} + z\left\{k\right\} \quad (29)$$

Where

$$\left\{\varepsilon^0\right\} = \begin{Bmatrix} \frac{\partial u_x^0}{\partial x} \\ \frac{\partial u_y^0}{\partial x} \\ \left[\frac{\partial u_x^0}{\partial y} + \frac{\partial u_y^0}{\partial x}\right] \end{Bmatrix}. \quad (30)$$

And

$$\left\{k\right\} = \begin{bmatrix} k_{xx} \\ k_{yy} \\ k_{xy} \end{bmatrix} = \begin{bmatrix} \frac{-\partial^2 u_z}{\partial x^2} \\ \frac{-\partial^2 u_z}{\partial y^2} \\ \frac{-2\partial^2 u_x}{\partial x \partial y} \end{bmatrix}. \quad (31)$$

The strain at any point in the plate is defined as the sum of a mid-surface strain $\{\varepsilon^0\}$, and a curvature $\{\kappa\}$ multiplied by the distance from the mid-surface.

The terms 'k_{xx}' and 'k_{yy}' are the bending moment curvatures and 'k_{xy}' is the twisting moment curvature. The midplane strains 'ε_{xy}^0' and the curvatures 'k_{xy}' are independent of 'z' location. It is obvious that the strains are continuous through the thickness of the laminate and vary linearly [8].

3.8. Stresss and Moment Resultants

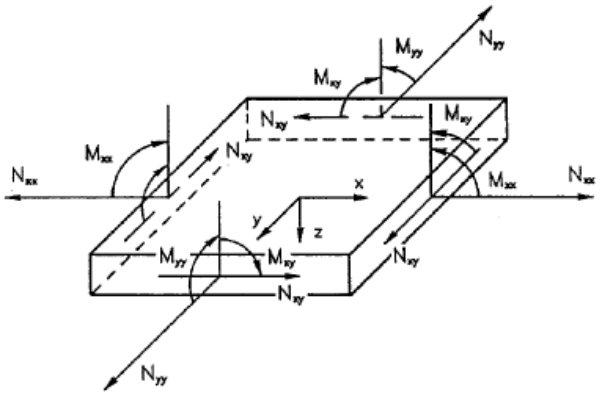

Figure 3. Stress and Moment Resultants.

The stress resultants are defined as;

$$\{N\} = \begin{bmatrix} N_{xx} \\ N_{yy} \\ N_{xy} \end{bmatrix} = \int_{-h}^{h} \{\sigma_x\}\, dz. \tag{32}$$

And the moment resultants are defined as

$$\{M\} = \begin{bmatrix} M_{xx} \\ M_{yy} \\ M_{xy} \end{bmatrix} = \int_{-h}^{h} \{\sigma_x\}\, z dz. \tag{33}$$

The integrations are carried out over the plate thickness.

Equations (11) and (29) can be used to express relationships in equations (32) and (33) as;

$$\{N\} = \int_{-h}^{h} \{\sigma_x\}\, dz = \int_{-h}^{h} \left[\bar{Q}\right]\left(\left\{\varepsilon^0\right\} + z\{k\}\right) dz \tag{34}$$

and

$$\{M\} = \int_{-h}^{h} \{\sigma_x\}\, dz = \int_{-h}^{h} \left[\bar{Q}\right]\left(\left\{\varepsilon^0\right\} + z\{k\}\right) z dz. \tag{35}$$

Since the transformed lamina stiffness matrices are constant within each lamina and the mid-plane strains and curvatures are constant with respect to the z-coordinate, the integrals in Equations (34) and (35) can be replaced by summations.

Introducing three matrices equivalent to the necessary summations, the relations can be written as;

$$\{N\} = [A]\left\{\varepsilon^0\right\} + [B]\{k\} \tag{36}$$

$$\{M\} = [B]\left\{\varepsilon^0\right\} + [D]\{k\}. \tag{37}$$

Obviously, the stiffness matrix is composed of the following 3 × 3 matrices

$$[A] = \sum_{i=1}^{n} \left[\bar{Q}\right]^i \left(z_i - z_{i-1}\right) \tag{38}$$

$$[B] = \tfrac{1}{2} \sum_{i=1}^{n} \left[\bar{Q}\right]^i \left(z_i^2 - z_{i-1}^2\right) \tag{39}$$

$$[D] = \tfrac{1}{3} \sum_{i}^{n} \left[\bar{Q}\right]^i \left(z_i^3 - z_{i-1}^3\right). \tag{40}$$

The reduced lamina stiffnesses for the ith ply are found in equations (36) and (37) using the principal properties and orientation angle for each ply in turn. Thus, the constitutive relations for a laminate have been developed in terms of stress and moment resultants.

The combined influence of various types of loads and moments on laminated plate response can be described using the ABD matrix from equations (36) and (37). In combined form:

$$\begin{bmatrix} N_x \\ N_y \\ N_{xy} \\ M_x \\ M_y \\ M_{xy} \end{bmatrix} = \begin{bmatrix} A_{11} & A_{12} & A_{16} & B_{11} & B_{12} & B_{16} \\ A_{21} & A_{22} & A_{26} & B_{21} & B_{22} & B_{26} \\ A_{61} & A_{62} & A_{66} & B_{61} & B_{62} & B_{66} \\ B_{11} & B_{12} & B_{16} & D_{11} & D_{12} & D_{16} \\ B_{21} & B_{22} & B_{26} & D_{21} & D_{22} & D_{26} \\ B_{61} & B_{62} & B_{66} & D_{61} & D_{62} & D_{66} \end{bmatrix} \begin{Bmatrix} \varepsilon_x \\ \varepsilon_y \\ \varepsilon_{xy} \\ k_x \\ k_y \\ k_{xy} \end{Bmatrix}. \tag{41}$$

3.9. ANSYS Mechanical APDL Design for Wing Skin

Governing Equations for Shell Element Behaviour in ANSYS

The relevant matrix equations are defined by [3];

$$\begin{Bmatrix} N \\ M \end{Bmatrix} = \begin{Bmatrix} A & B \\ B^T & D \end{Bmatrix} \begin{Bmatrix} \varepsilon \\ k \end{Bmatrix} - \left(T - T^1\right) \begin{Bmatrix} M^T \\ B^T \end{Bmatrix} \tag{42}$$

$$[S] = [E]\{\gamma\}, \tag{43}$$

Where; γ is the stress tensor.

3.10. Analytical Modeling of Wing Load

There are three primary loads that acts on the aircraft wing [2]: aerodynamic lift, load due to structure weight and load due to the fuel contained in the wing. These loads act perpendicularly to the wing surface and their magnitude varies along the length of the wing [2].

The total load can be obtained by adding the three individual load components. This analytical model gives a clear view of how aircraft weight and geometry parameters affect total load, i.e.;

$$q_t(x) = q_l(x) + q_w(x) + q_f(x) \tag{44}$$

$$q_t(x) = \begin{cases} \dfrac{n\left(\begin{matrix} 2C_o W t_o \sqrt{L^2 - x^2} + 2C_t W t_o \sqrt{L^2 - x^2} \\ -\pi C_o L\ Wws + \pi C_o Wws\ x - \pi C_t Wws\ x \end{matrix}\right)}{L^2 \pi \left(C_o + C_t\right)} \\ \quad if\ Lf < x \\ \dfrac{2Wt_o n\sqrt{L^2 - x^2}}{L^2 \pi} - \dfrac{Wws\ n\left(C_t x - C_o x + C_o L\right)}{L^2 \left(C_o + C_t\right)} \\ -\dfrac{Wf\ n\left(C_t f\ x - C_o f\ x + C_o f\ Lf\right)}{Lf^2 \left(C_o f + C_t f\right)}\ if\ Lf \geq x. \end{cases} \tag{45}$$

Shear force along the wing is derived by integrating the total load [2,7].

4. Materials, Equipment and Methods

4.1. Materials

The major materials used for this research work are:
i. Low Modulus Graphite-Epoxy Lamina.
ii. High Modulus Graphite-Epoxy Lamina.
iii. Ultra Modulus Graphite-Epoxy Lamina.
The design properties employed are reflected in Table 1 to Table 4 below:
(a) Low Modulus (LM) Graphite-Epoxy Lamina.

Table 1. Design Values for Low Modulus (LM) Graphite-Epoxy Composite

Material Properties	Value
Thickness (m)	0.00023
E_{11} (N/m^2)	1.44790E+11
E_{22} (N/m^2)	9.65266E+09
E_{33} (N/m^2)	9.65266E+09
$NU_{12(xy)}$	2.5E-01
$NU_{23(yz)}$	4.065E-01
$NU_{13(xz)}$	2.5E-01
$G_{12(xy)}$	5.86054E+09
$G_{23(yz)}$	3.46117E+09
$G_{13(xz)}$	5.86054E+09
Density (Kg/m^3)	1577.75

Source: Lamina Data of Autodesk Simulation Composite Design 2015 Software.

(b) High Modulus (HM) Graphite-Epoxy Lamina.

Table 2. Design Values for High Modulus (HM) Graphite-Epoxy Composite.

Material Properties	Value
Thickness (m)	0.00023
E_{11} (N/m^2)	2.20632E+11
E_{22} (N/m^2)	6.89476E+09
E_{33} (N/m^2)	6.89476E+09
$NU_{12(xy)}$	2.5E-01
$NU_{23(yz)}$	4.103E-01
$NU_{13(xz)}$	2.5E-01
$G_{12(xy)}$	4.82633E+09
$G_{23(yz)}$	2.71653E+09
$G_{13(xz)}$	4.82633E+09
Density (Kg/m^3)	1633.11

Source: Lamina Data of Autodesk Simulation Composite Design 2015 Software.

(c) Ultra Modulus (UM) Graphite-Epoxy Lamina.

Table 3. Design Values for Ultra Modulus (UM) Graphite-Epoxy Composite.

Material Properties	Value
Thickness (m)	0.00023
E_{11} (N/m^2)	2.89580E+11
E_{22} (N/m^2)	6.20528E+09
E_{33} (N/m^2)	6.20528E+09
$NU_{12(xy)}$	2.5E-01
$NU_{23(yz)}$	4.197E-01
$NU_{13(xz)}$	2.5E-01
$G_{12(xy)}$	4.82633E+09
$G_{23(yz)}$	2.65586E+09
$G_{13(xz)}$	4.82633E+09
Density (Kg/m^3)	1688.47

Source: Lamina Data of Autodesk Simulation Composite Design 2015 Software.

(d) Wing Design Properties: Aerofoil Model NACA 2415 for the wing of a small passenger aircraft.

Table 4. Aircraft and Visualize Wing Loads Parameters

S/N	Wing Design Parameters	Value
1	Total aircraft weight (Wto)	4,800kg
2	Weight of wing structure (Wws)	630kg
3	Weight of fuel stored in wing (Wf)	675kg
4	Length of wing (L)	7m
5	Length of fuel tank within wing (Lf)	2.4m
6	Chord length of wing root (Co)	1.8m
7	Chord length of wing tip (Ct)	1.4m
8	Width of fuel tank at wing root (Cof)	1.1m
9	Width of fuel tank at wing tip (Ctf)	0.85m
10	Load factor (n)	1.5

4.2. Equipment

The equipment used in this work is an Hp Compaq 615 personal computer.The following software applications below were employed to carry out the various analyses:

i. MATLAB R2016a (9.0.0.341360) Software, by MathWorks, Inc.
ii. Autodesk Simulation Composite Design 2015, Version 2015.0.83417.111 by Autodesk, Inc.
iii. ANSYS 14 Mechanical APDL Software, by ANSYS Inc. USA.

4.3. Methods

The aircraft loads were modeled using MATLAB and symbolic Math Toolbox called MuPAD to determine the shear loads on the wing of a small passenger aircraft. This was carried out with the aim of ascertaining whether the proposed designs meet strength requirements.

Thereafter, predictive behaviour of the wing skin composite laminate designs was analyzed under shear loading condition through an easy-to-use graphical interface of the Autodesk Simulation Composite Design software.

The developed stresses and displacements under static loading conditions were analyzed for both the wing skin composite laminate designs using finite element methods with the help of ANSYS 14 Mechanical APDL.

5. Results, Analysis and Discussions

5.1. Results for Autodesk Simulation Composite Design

The summary of the designed results are shown in Table 5 – Table 7.

In Table 5, Table 6 and Table 7, the predictive analytical results between the two stacking sequences [(+/-45/0/90)s]n and [(+/-45)s]n showed that for any of the designs LM and HM, LM and UM, and HM and UM; [(+/-45)s]n stacking sequence showed better bending and stability properties while [(+/-45/0/90)s]n only demonstrated better vibrational property. Also, the realistic values showed that the various designs are feasible for further finite element analyses.

5.2. Results for Laminate Designs Using ANSYS Mechanical APDL for Finite Element Analyses.

The shear force distribution generated along the length of the wing was approximately 3,000N using MuPAD symbolic math tool in MATLAB [2].

5.2.1. Graphical Results of the Various Laminate Designs

The results of the various laminate designs covering the deflections, shear strain and Von Mises failure criteria are reflected in Figure 4 through Figure 33, to show which design best withstands the developed shear force.

Table 5. Results for LM Graphite-Epoxy and HM Graphite-Epoxy Laminate.

S/N	Laminate Analysis		[(+/-45/0/90)s]n	[(+/-45)s]n
1.	Bending	Deflection (mm)	1.39E+04	1.30E+04
		X-Moment (N-mm/mm)	8.43E+02	8.83E+02
		Y-Moment (N-mm/mm)	1.10E+03	1.09E+03
		XY-Moment (N-mm/mm)	-8.51E-31	-9.43E-31
2.	Stability (N/mm)		9.81E-02	1.05E-01
3.	Vibration (Hz)		1.65	1.71

Table 6. Results for LM Graphite-Epoxy and UM Graphite-Epoxy Laminate.

S/N	Laminate Analysis		[(+/-45/0/90)s]n	[(+/-45)s]n
1.	Bending	Deflection (mm)	1.25E+04	1.17E+04
		X-Moment (N-mm/mm)	8.54E+02	9.00E+02
		Y-Moment (N-mm/mm)	1.10E+03	1.08E+03
		XY-Moment (N-mm/mm)	-8.50E-31	-9.60E-31
2.	Stability (N/mm)		1.09E-01	1.16E-01
3.	Vibration (Hz)		1.73	1.79

Table 7. Results for HM Graphite-Epoxy and UM Graphite-Epoxy Laminate.

S/N	Laminate Analysis		[(+/-45/0/90)s]n	[(+/-45)s]n
1.	Bending	Deflection (mm)	1.04E+04	9.66E+03
		X-Moment (N-mm/mm)	9.01E+02	9.37E+02
		Y-Moment (N-mm/mm)	1.09E+03	1.08E+03
		XY-Moment (N-mm/mm)	-9.18E-31	-1.01E-30
2.	Stability (N/mm)		1.32E-01	1.42E-01
3.	Vibration (Hz)		1.88	1.95

5.2.2. Analyses of LM Graphite_Epoxy and HM Graphite_Epoxy Laminate Designs

i. (a)

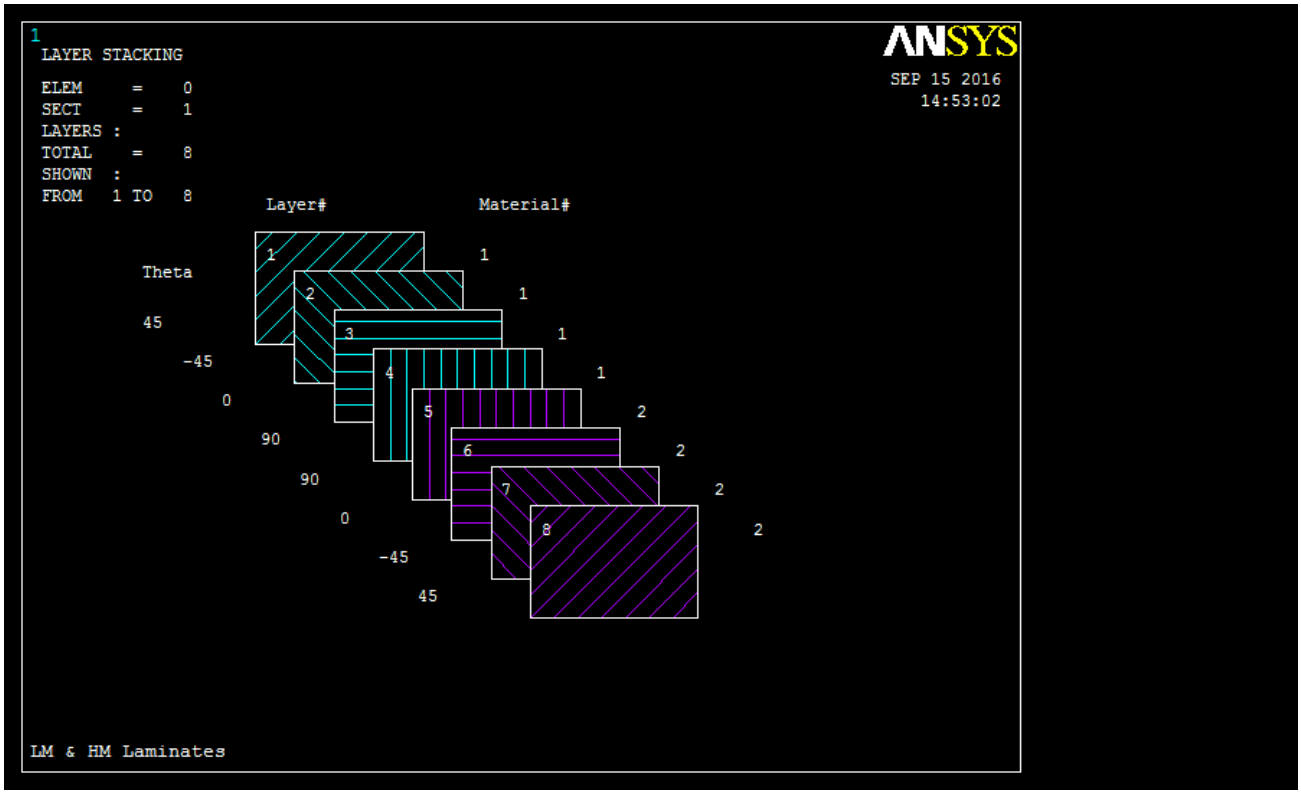

Figure 4. [(+/-45/0/90)s]n LM & HM Laminate Design Stacking Sequence

(b)

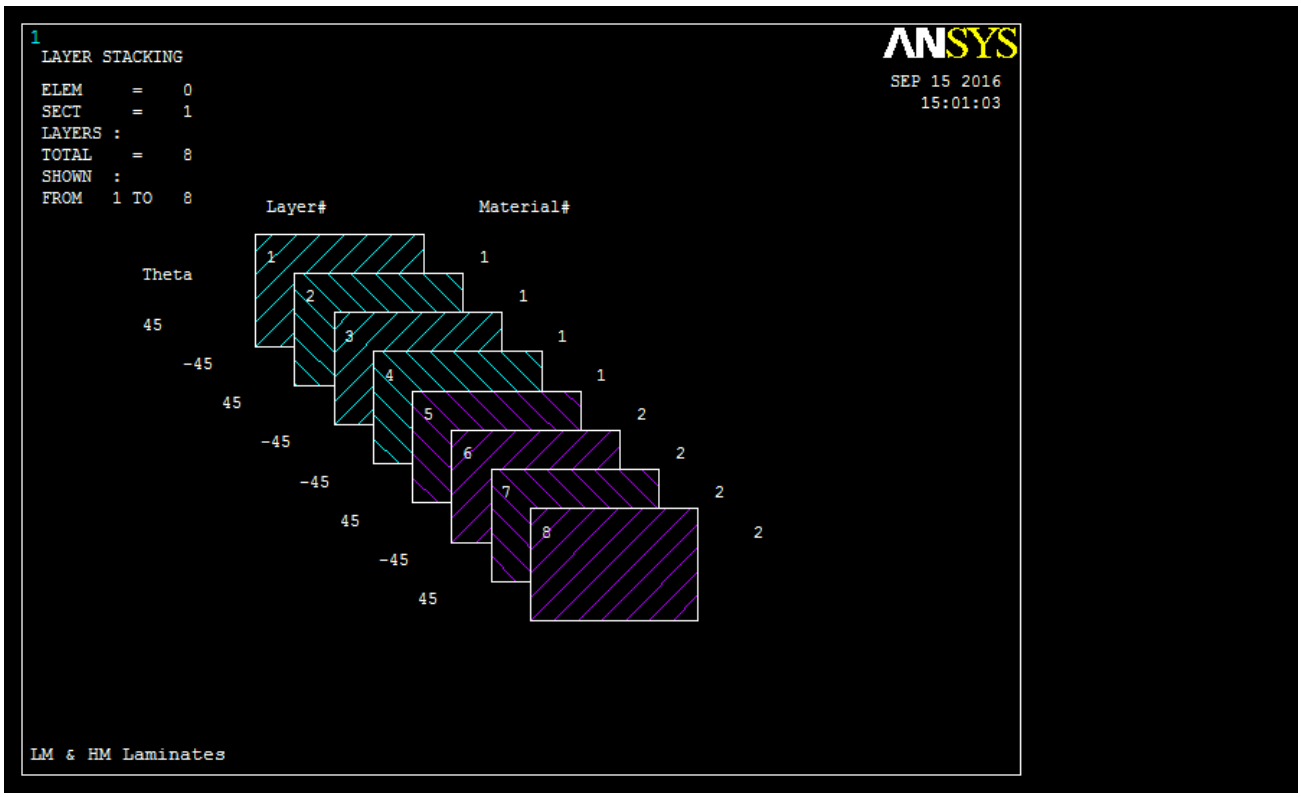

Figure 5. [(+/-45)s]n LM & HM Laminate Design Stacking Sequence

ii. (a)

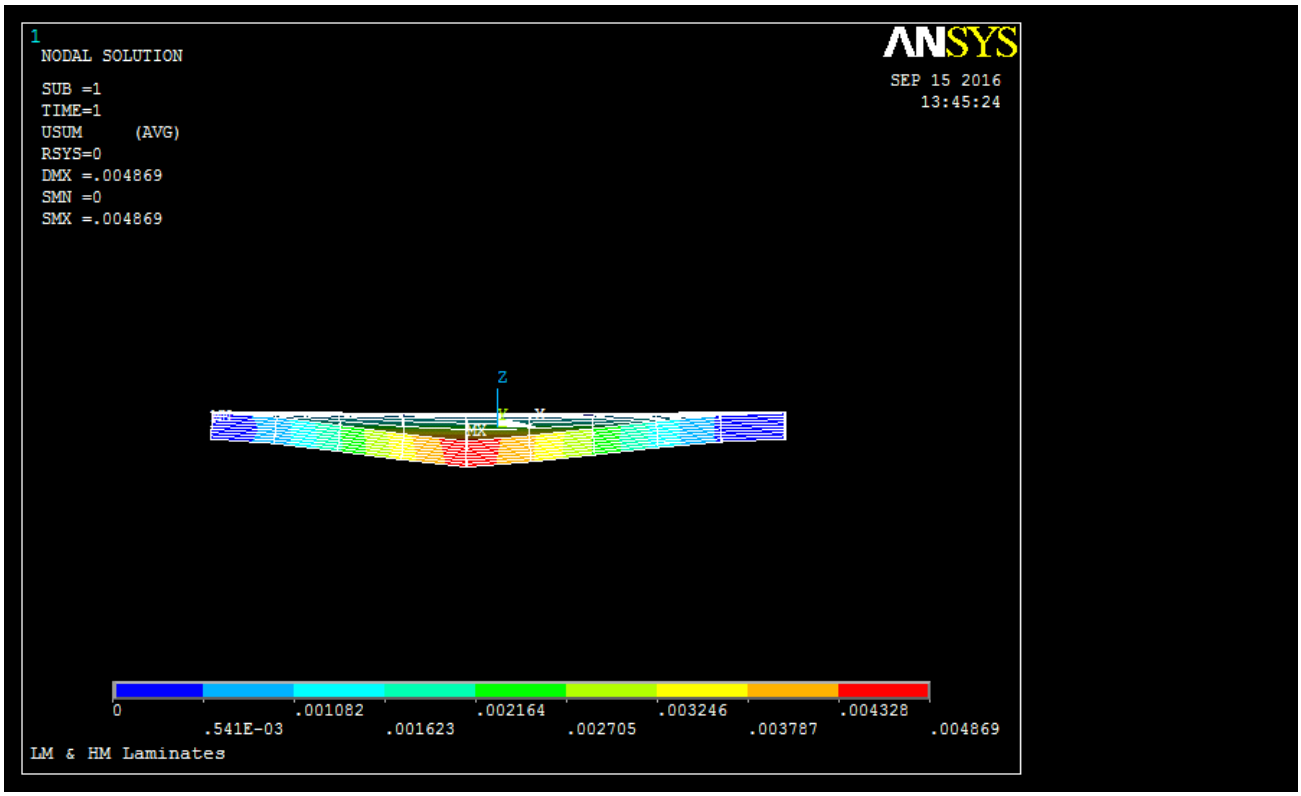

Figure 6. Deflection of [(+/-45/0/90)s]n Laminate Design.

(b)

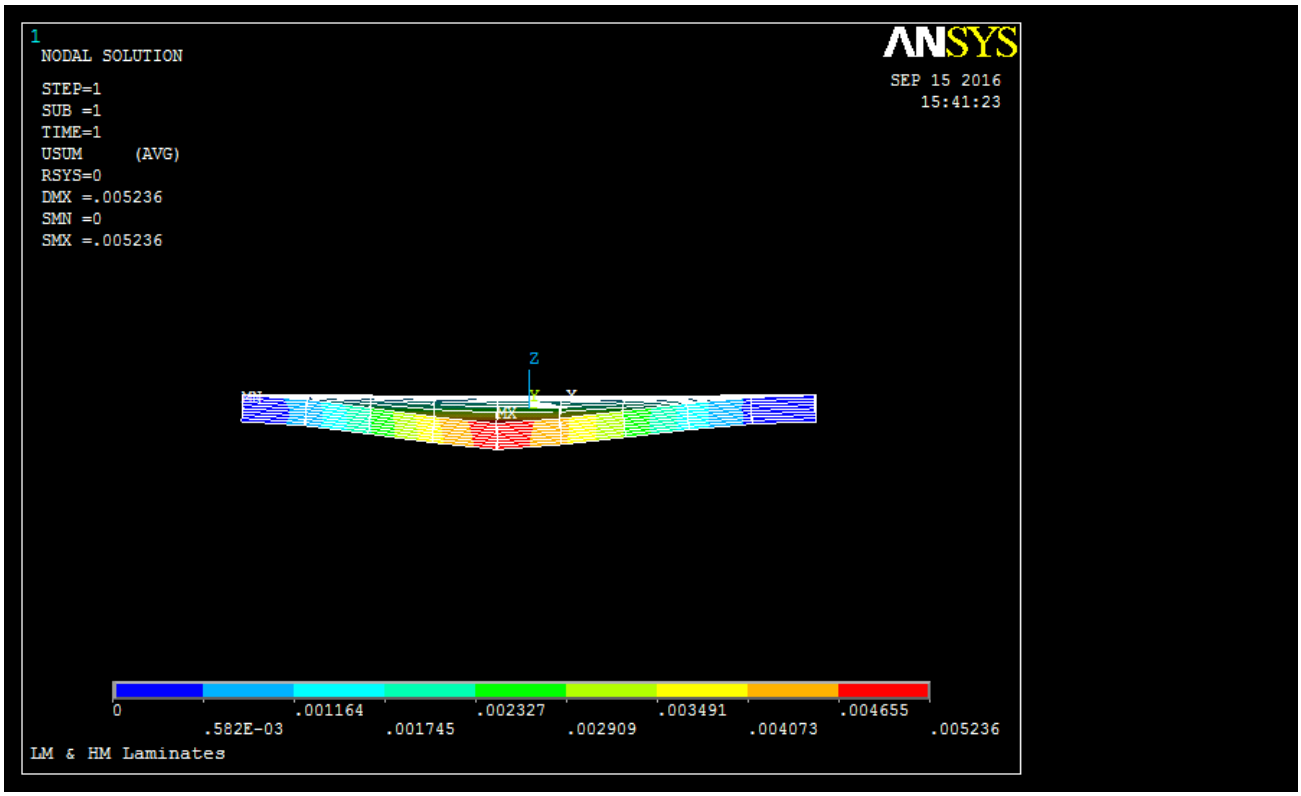

Figure 7. Deflection of [(+/-45)s]n Laminate Design.

iii. (a)

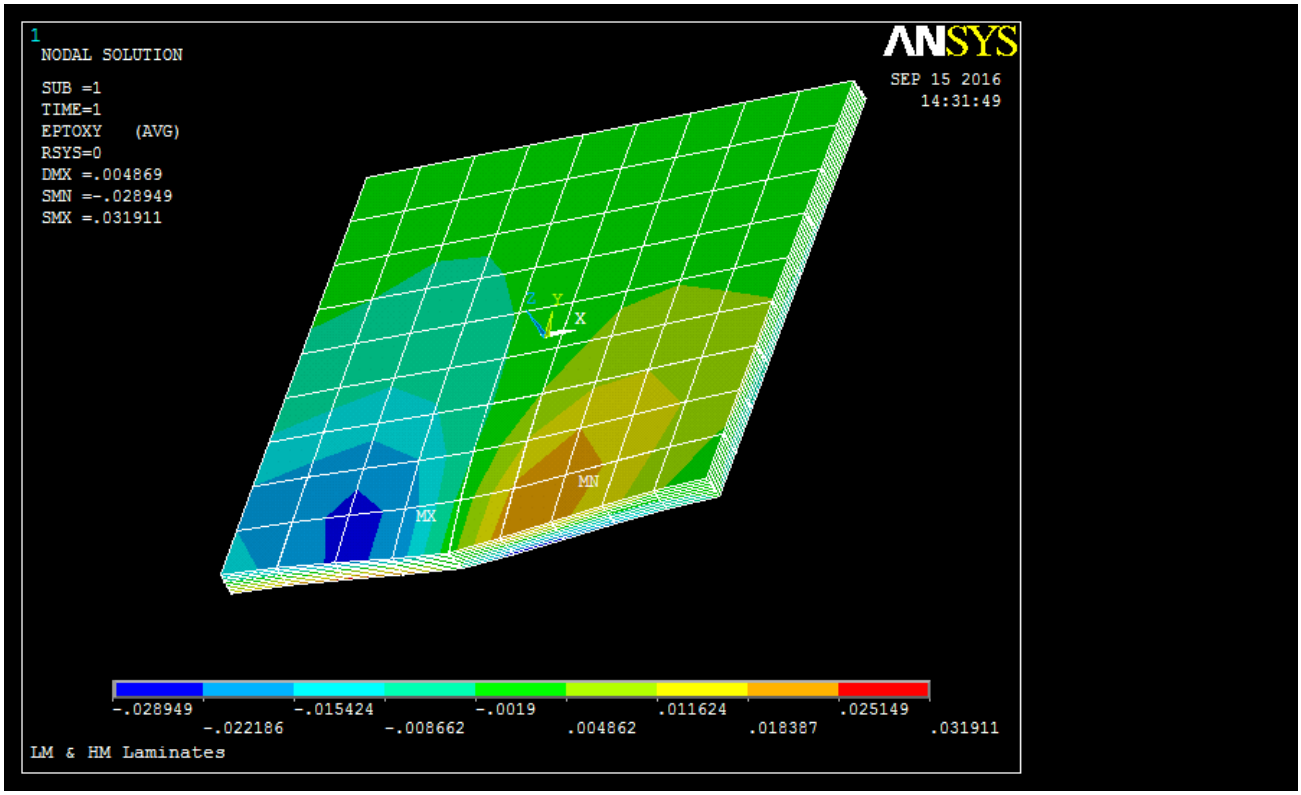

Figure 8. XY Shear Total Mechanical Strain of [(+/-45/0/90)s]n Laminate Design.

(b)

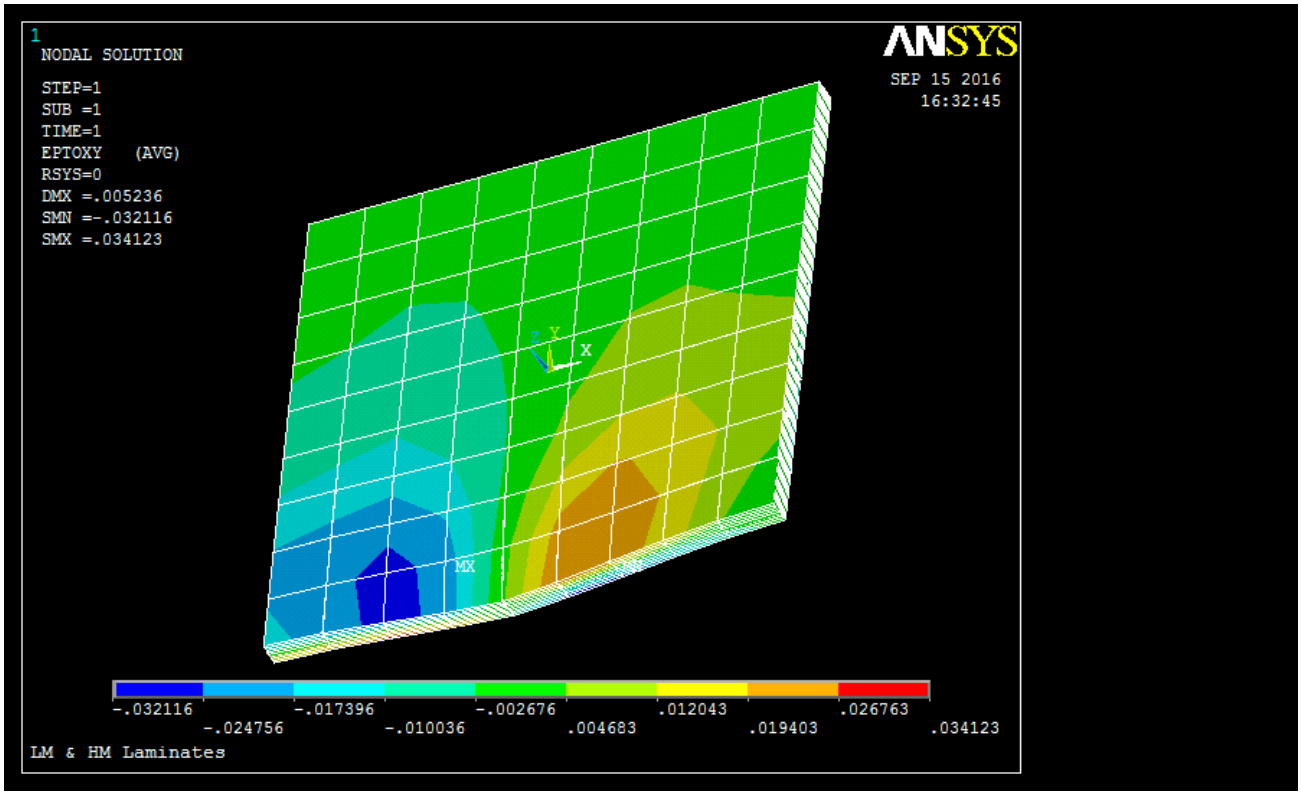

Figure 9. XY Shear Total Mechanical Strain of [(+/-45)s]n Laminate Design.

iv. (a)

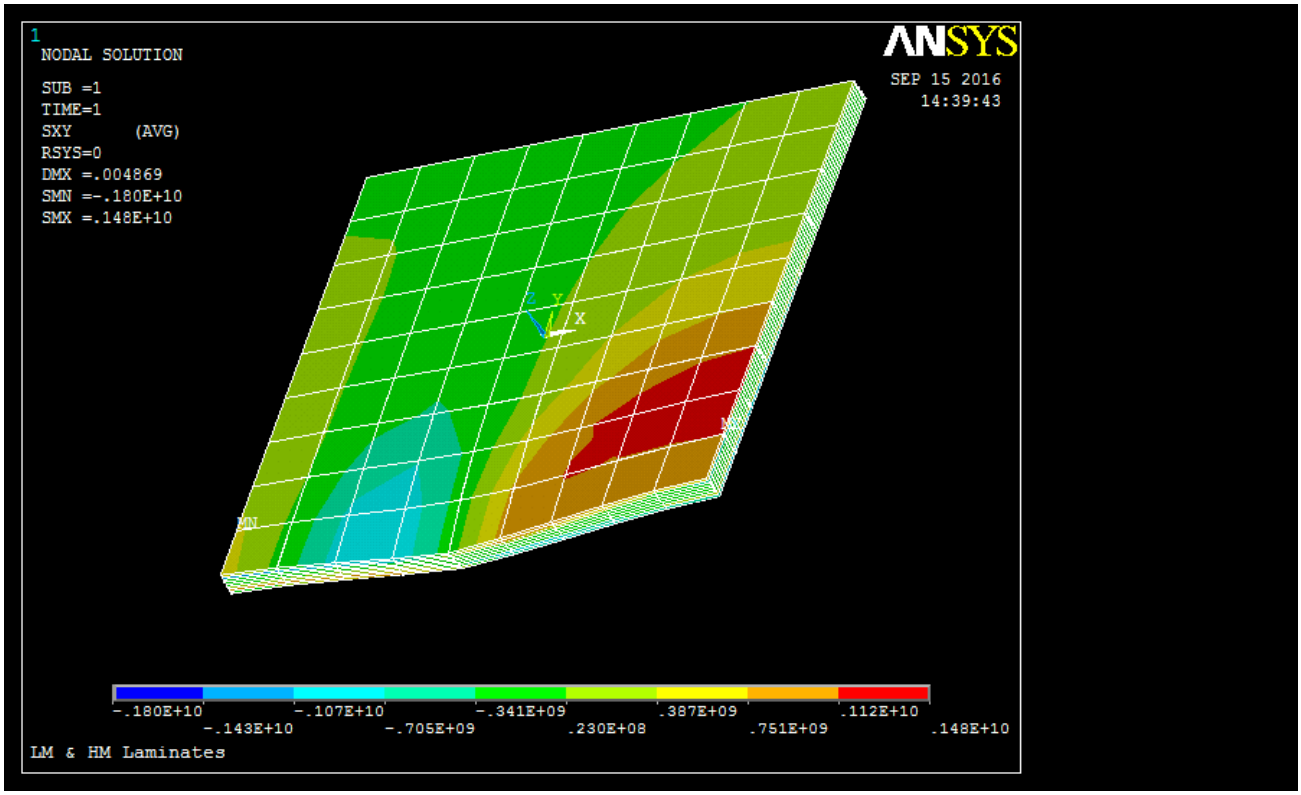

Figure 10. XY Shear Stress of [(+/-45/0/90)s]n Laminate Design.

(b)

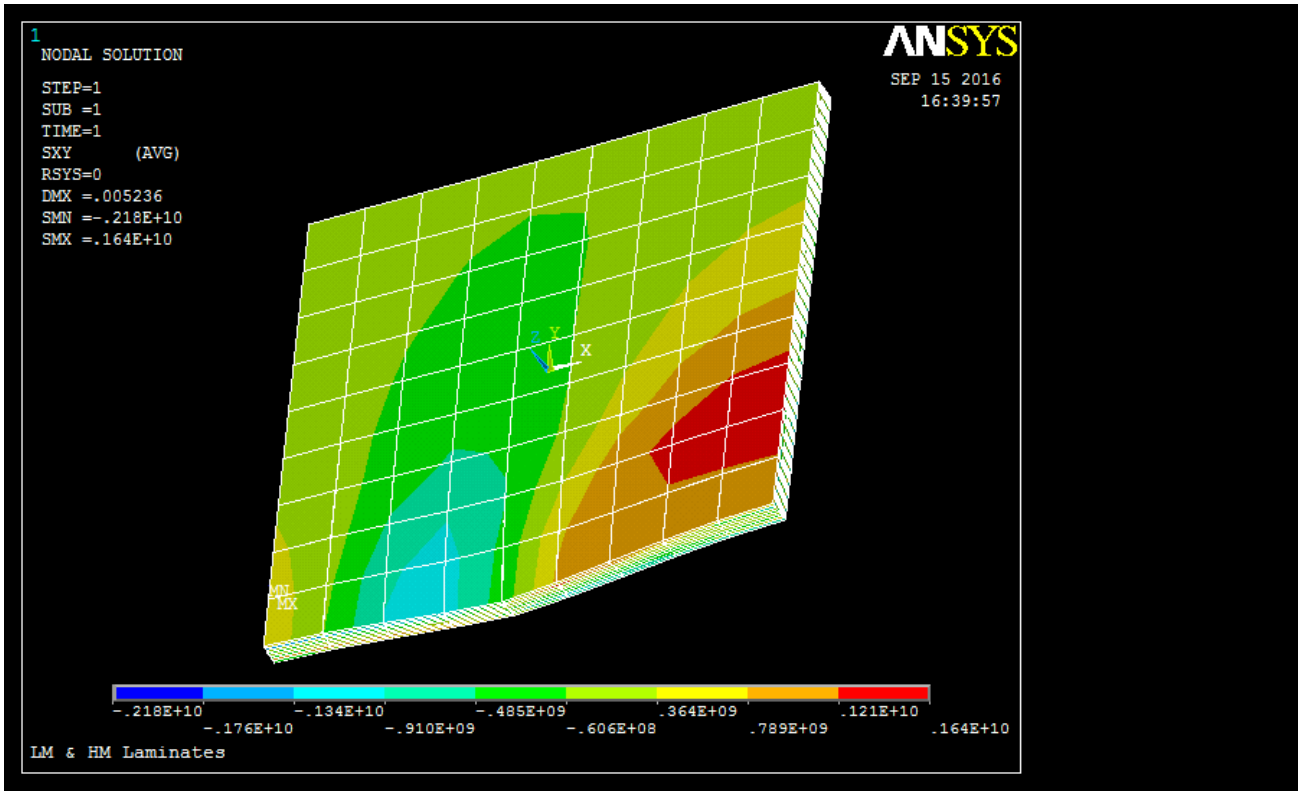

Figure 11. XY Shear Stress of [(+/-45)s]n Laminate Design.

v. (a)

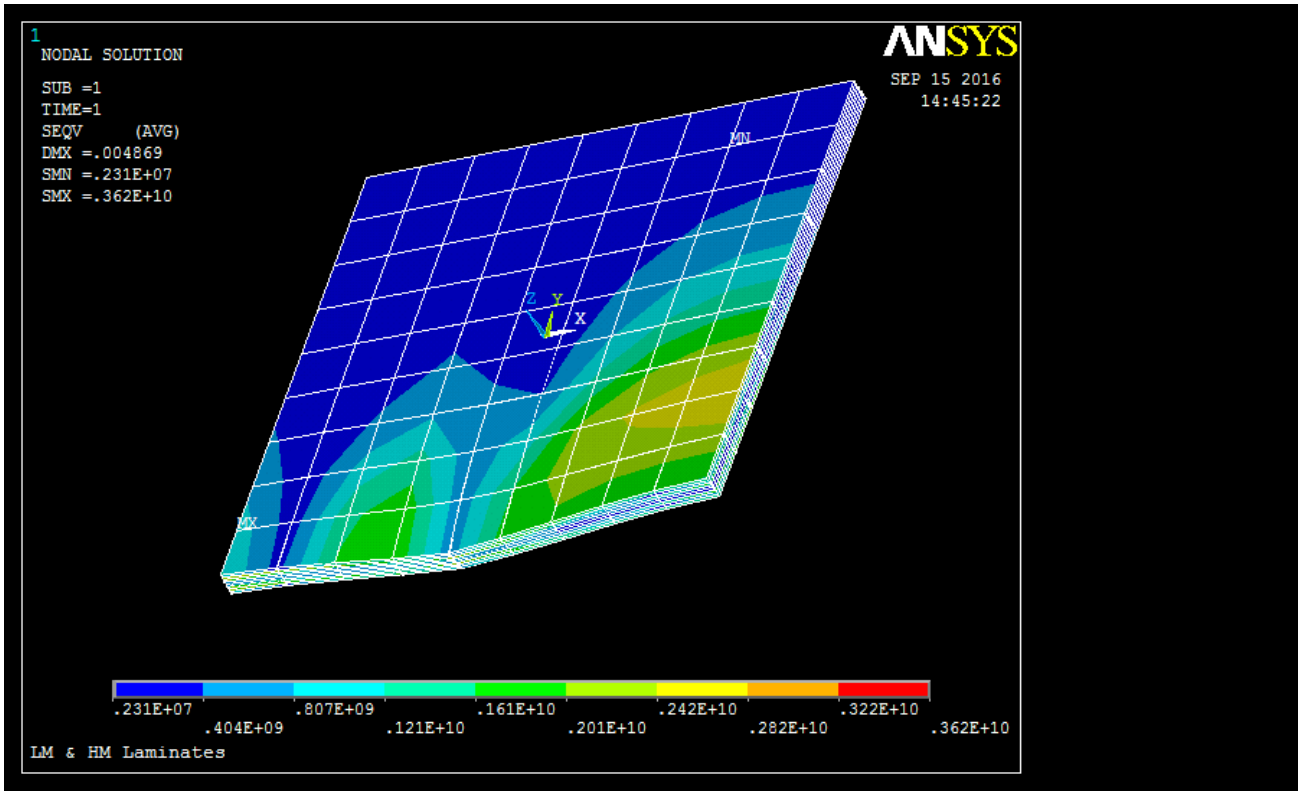

Figure 12. Von Mises Stress of [(+/-45/0/90)s]n Laminate Design.

(b)

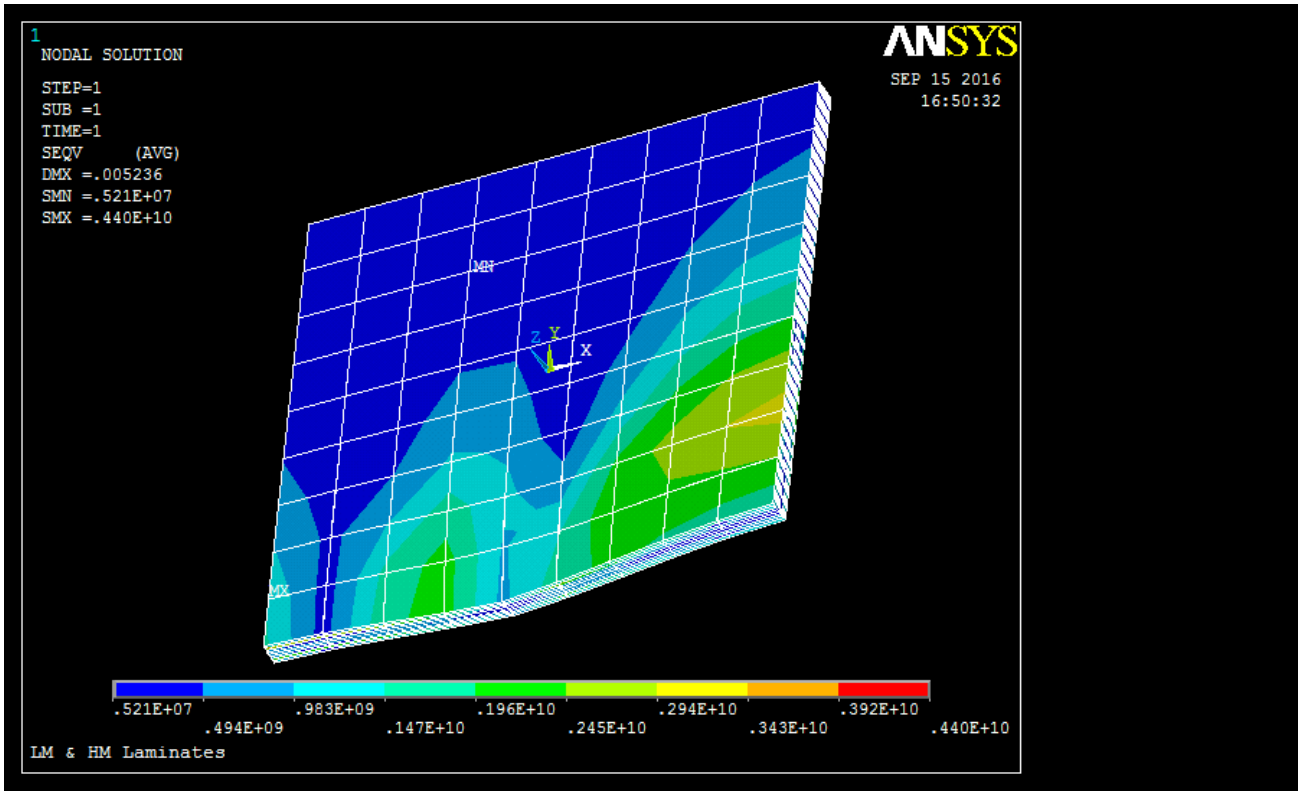

Figure 13. Von Mises Stress of [(+/-45)s]n Laminate Design.

5.2.3. Analyses of LM Graphite_Epoxy and UM Graphite_Epoxy Laminate Designs.

i. (a)

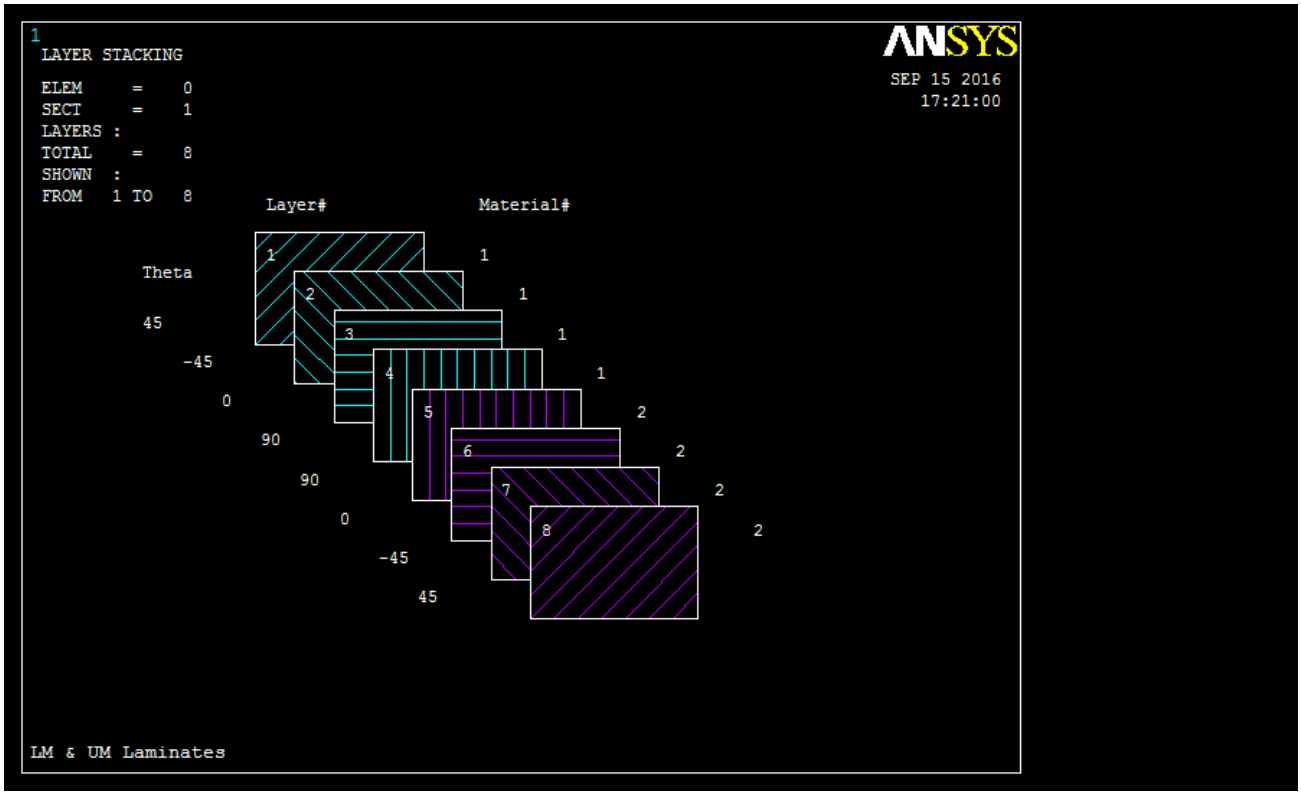

Figure 14. [(+/-45/0/90)s]n LM & UM Laminate Design Stacking Sequence.

(b)

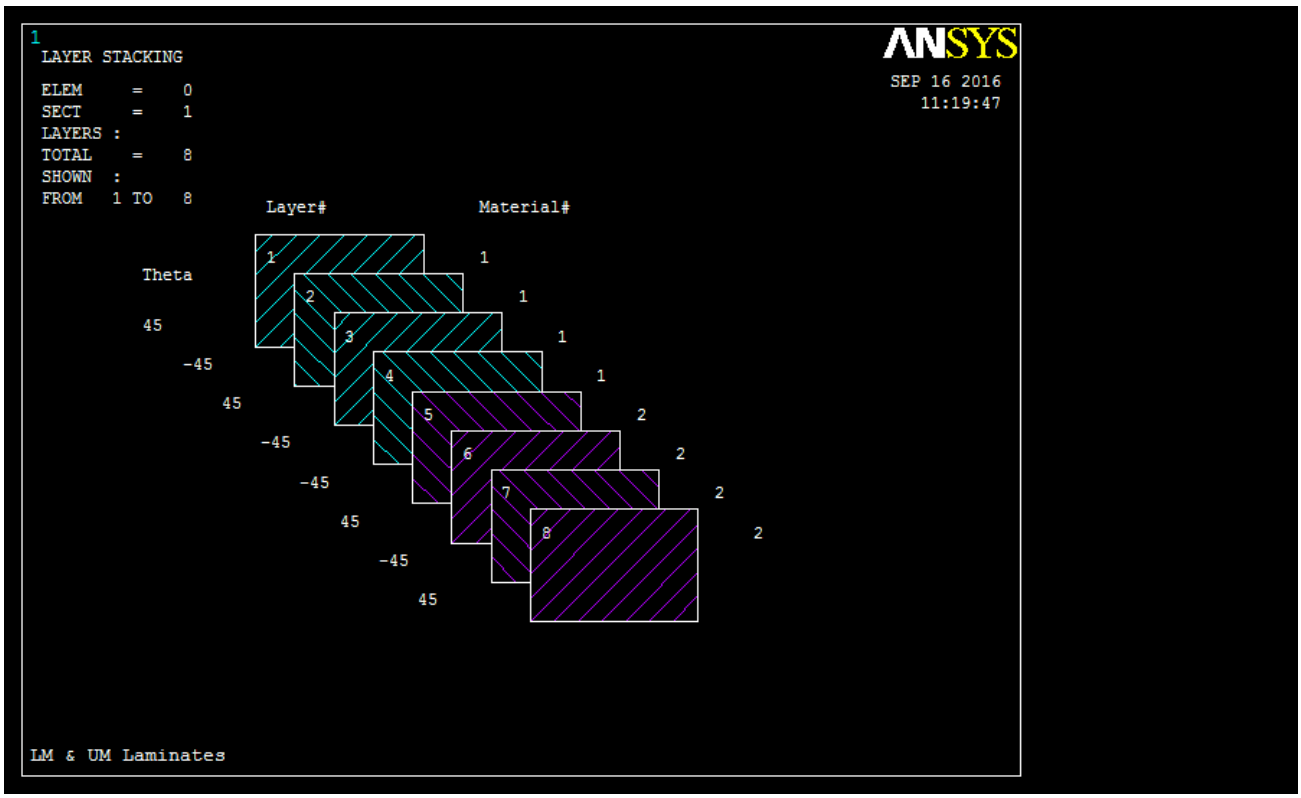

Figure 15. [(+/-45)s]n LM & UM Laminate Design Stacking Sequence.

ii. (a)

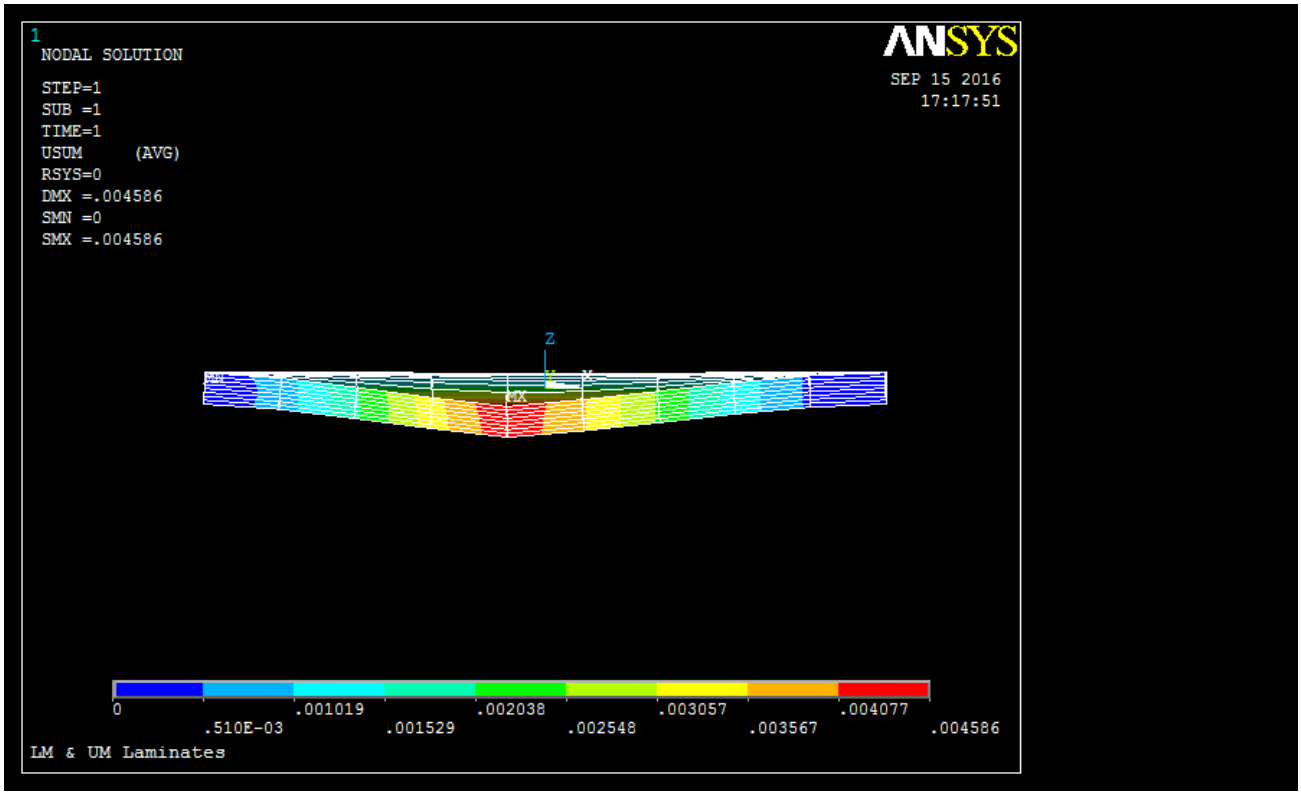

Figure 16. Deflection of LM & UM [(+/-45/0/90)s]n Laminate Design.

(b)

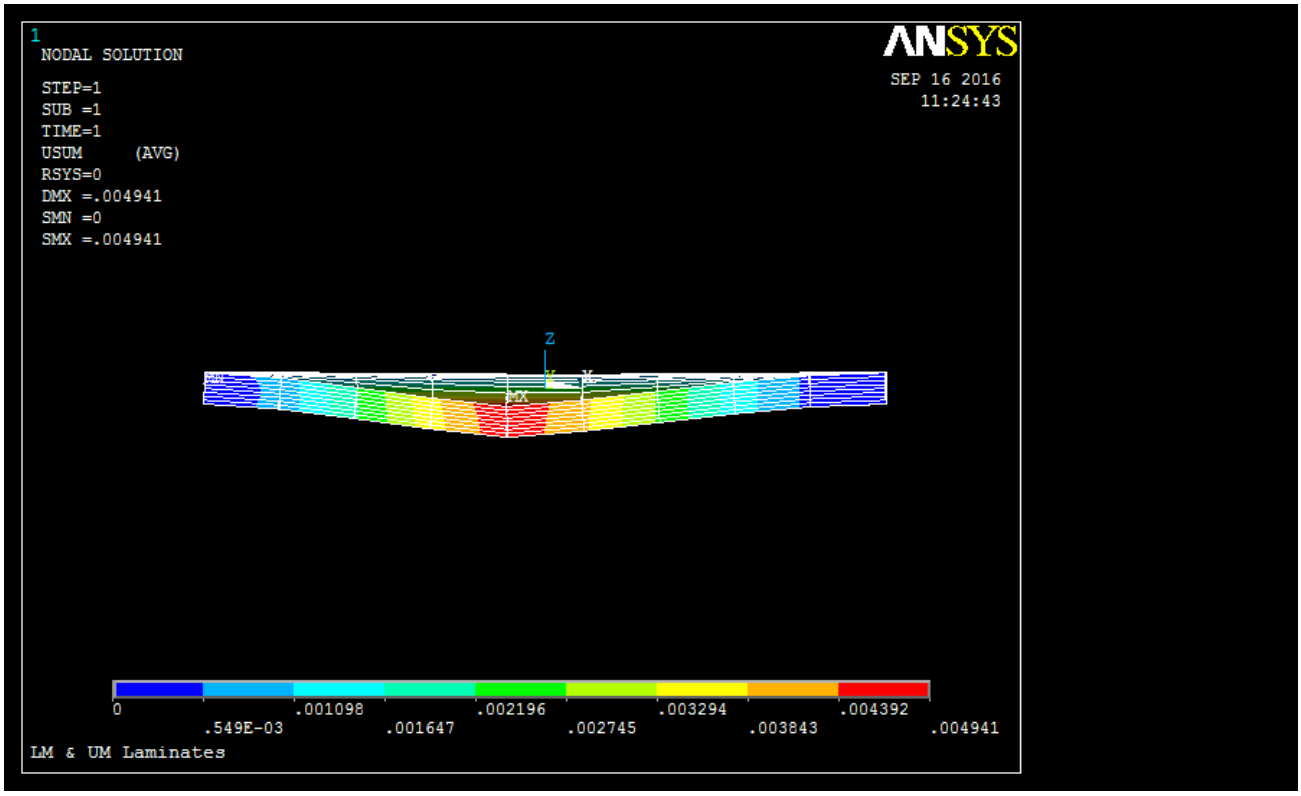

Figure 17. Deflection of LM & UM [(+/-45)s]n Laminate Design.

iii. (a)

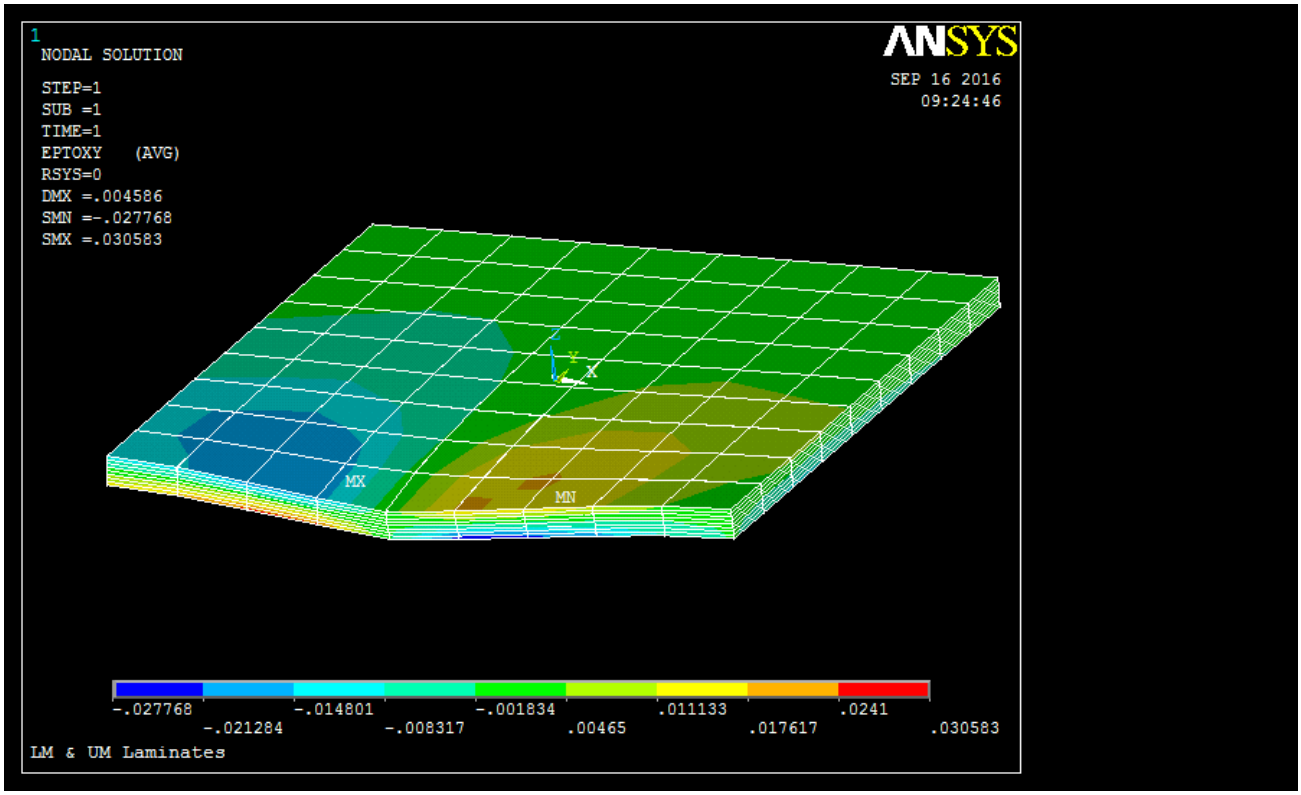

Figure 18. XY Shear Total Mechanical Strain of LM & UM [(+/-45/0/90)s]n Laminate Design.

(b)

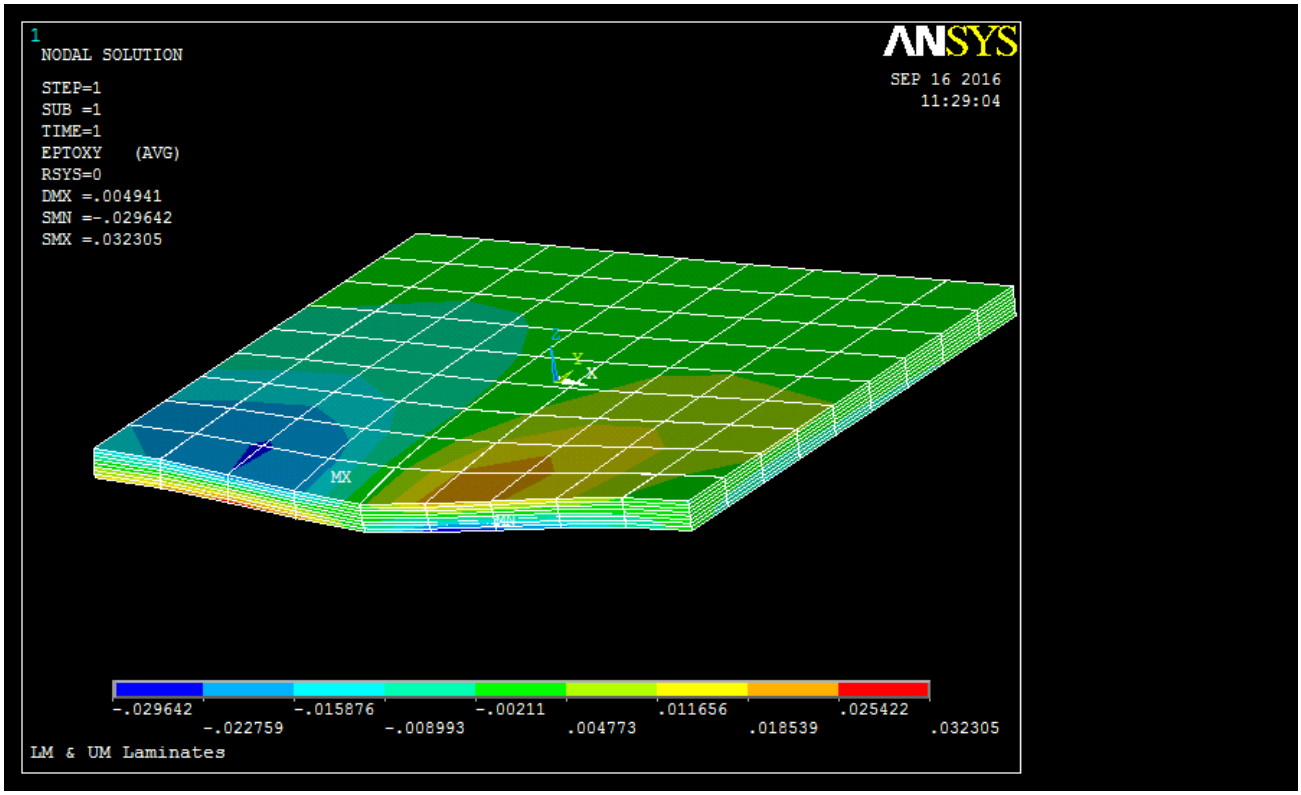

Figure 19. XY Shear Total Mechanical Strain of LM & UM [(+/-45)s]n Laminate Design

iv. (a)

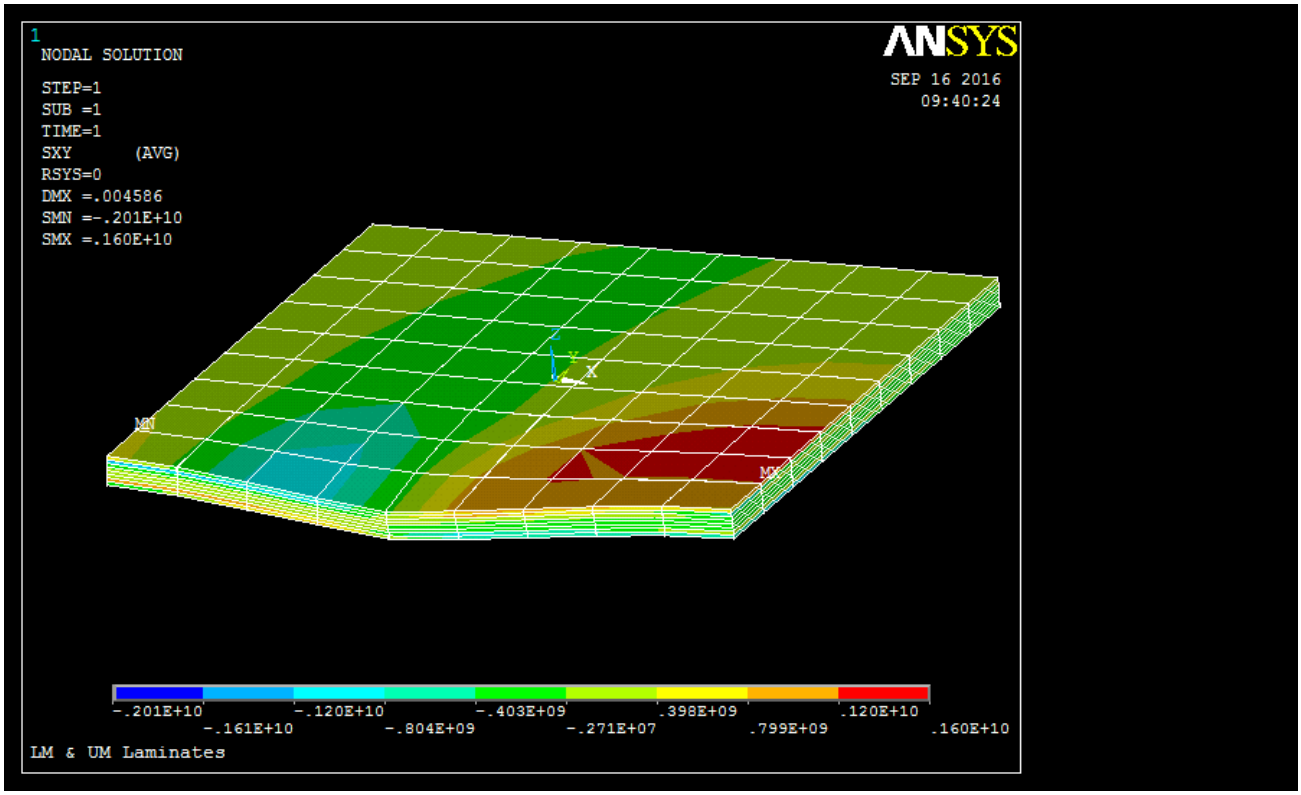

Figure 20. XY Shear Stress of LM & UM [(+/-45/0/90)s]n Laminate Design.

(b)

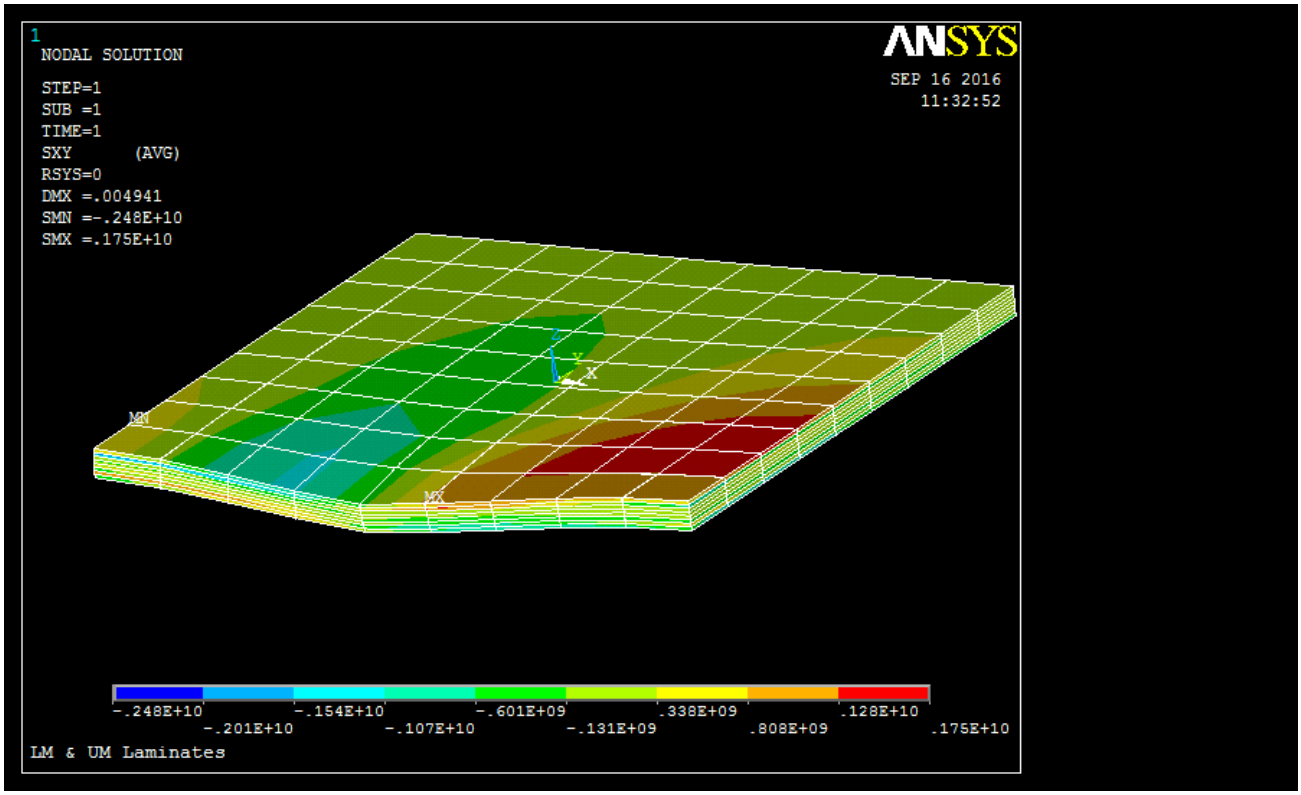

Figure 21. XY Shear Stress of LM & UM [(+/-45)s]n Laminate Design.

v. (a)

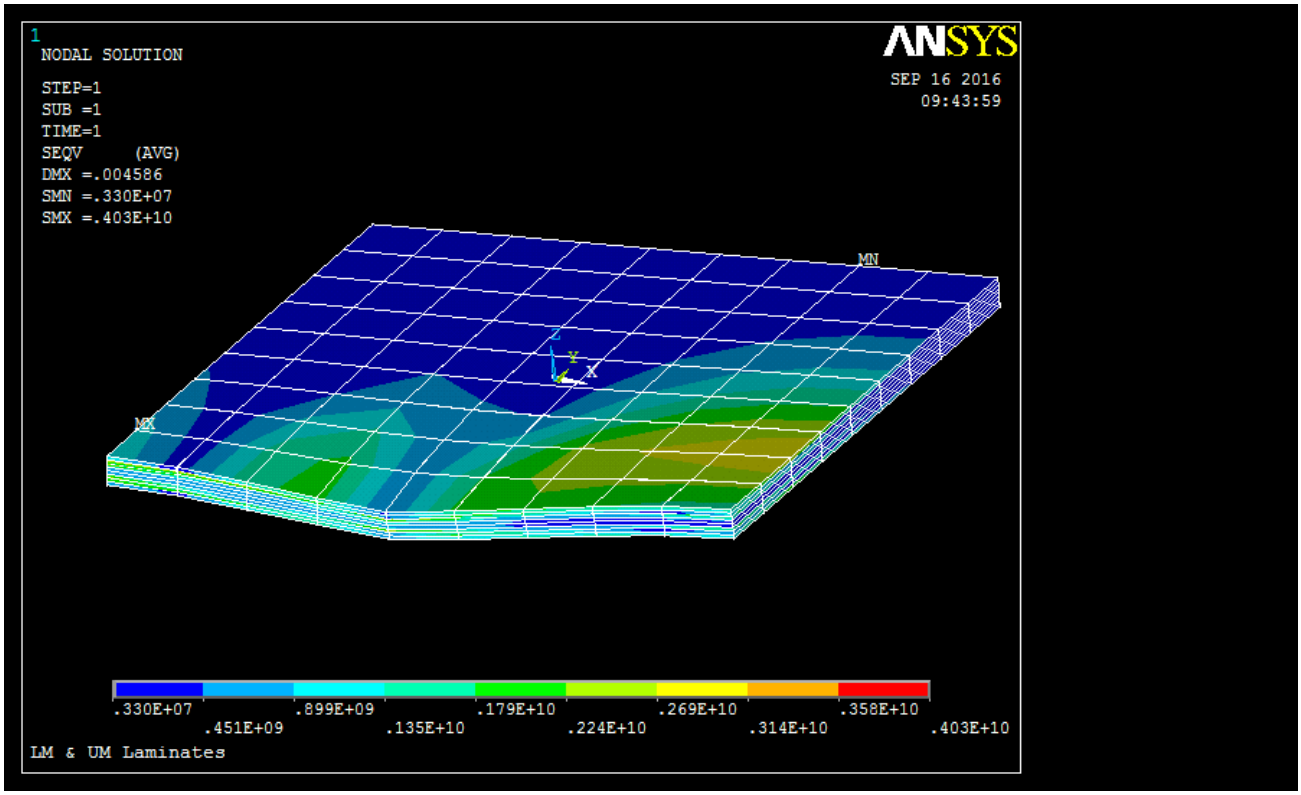

Figure 22. Von Mises Stress of LM & UM [(+/-45/0/90)s]n Laminate Design.

(b)

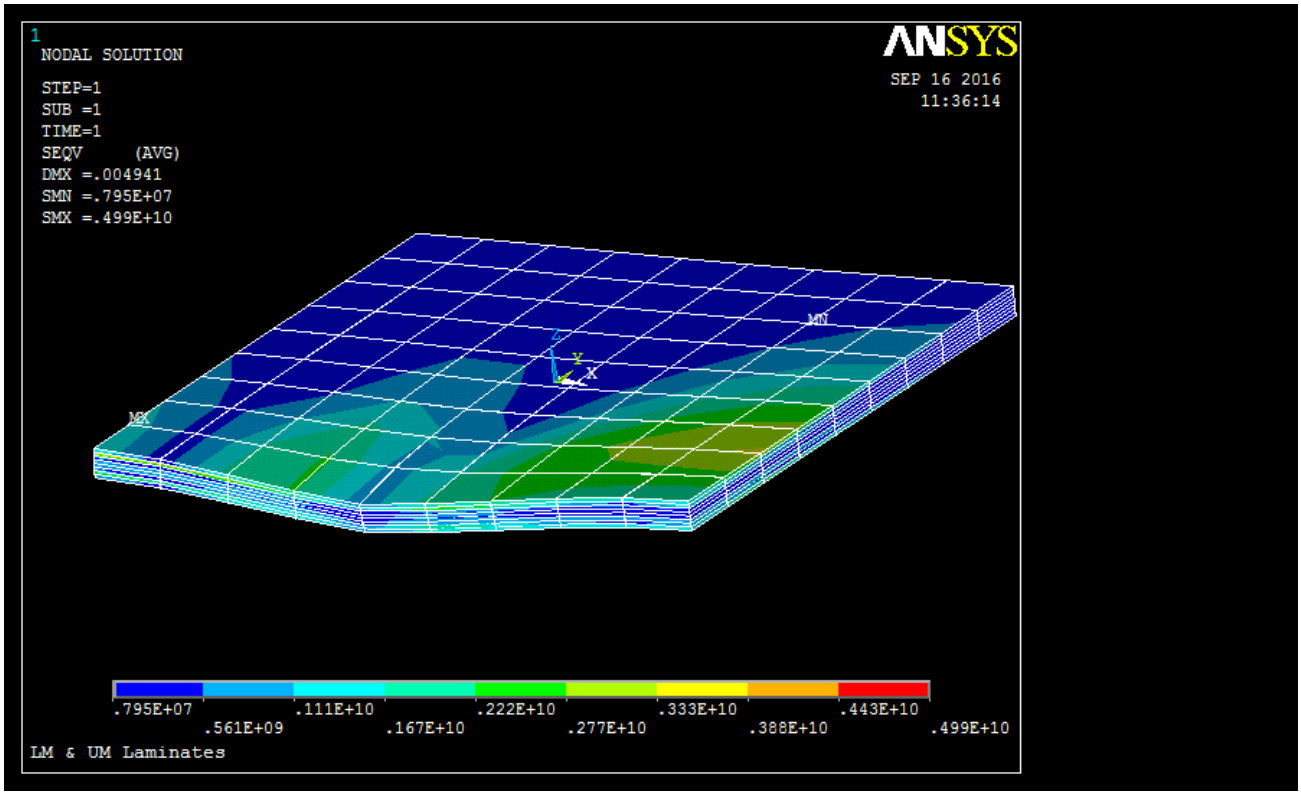

Figure 23. Von Mises Stress of LM & UM [(+/-45)s]n Laminate Design.

5.2.4. Analyses of HM Graphite_Epoxy and UM Graphite_Epoxy Laminate Designs.

i. (a)

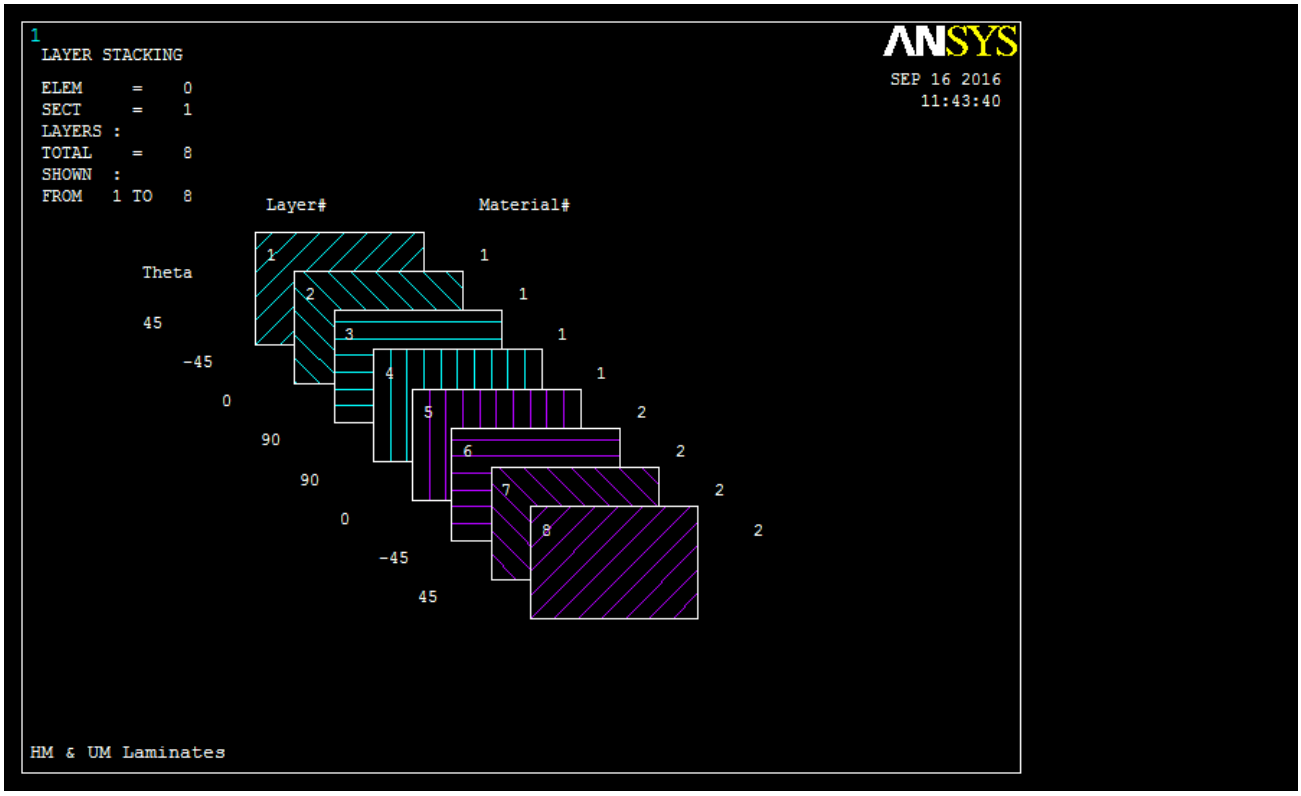

Figure 24. [(+/-45/0/90)s]n HM & UM Laminate Design Stacking Sequence.

(b)

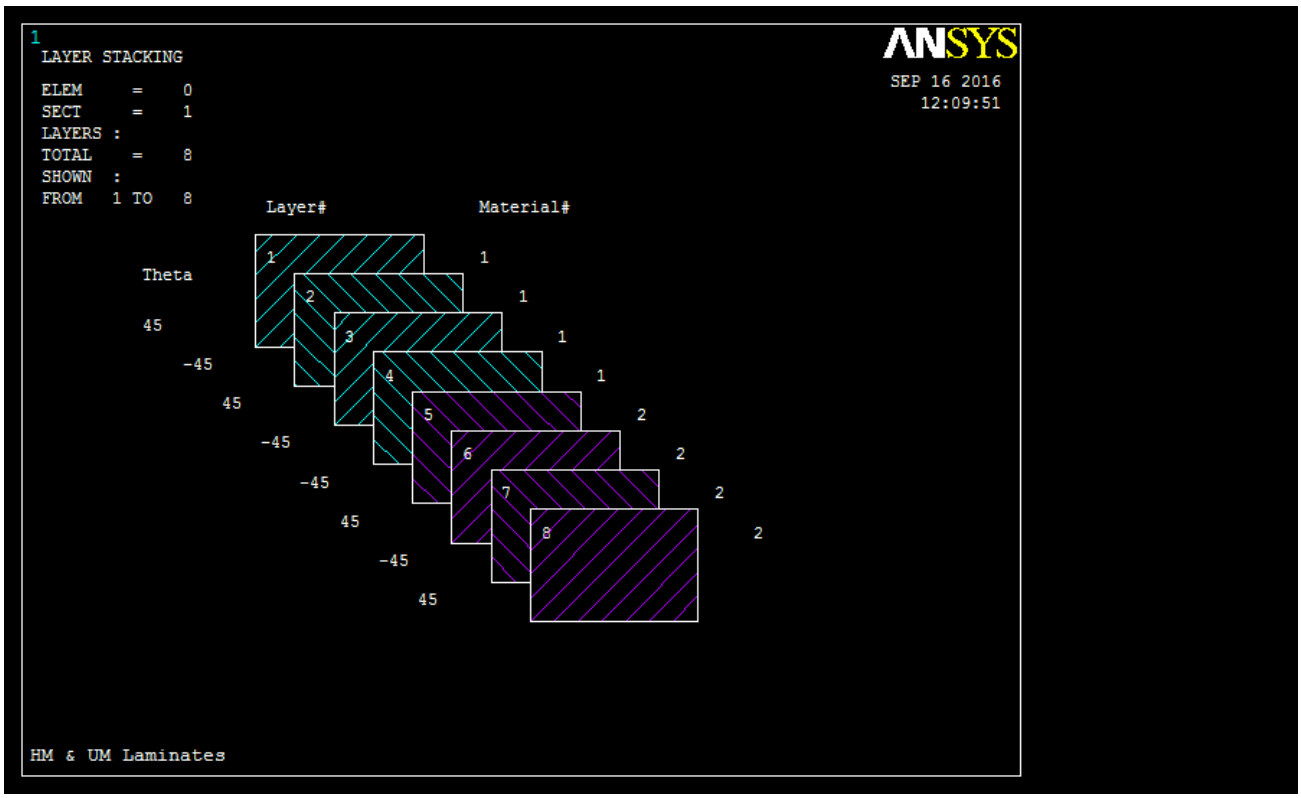

Figure 25. [(+/-45)s]n HM & UM Laminate Design Stacking Sequence.

ii. (a)

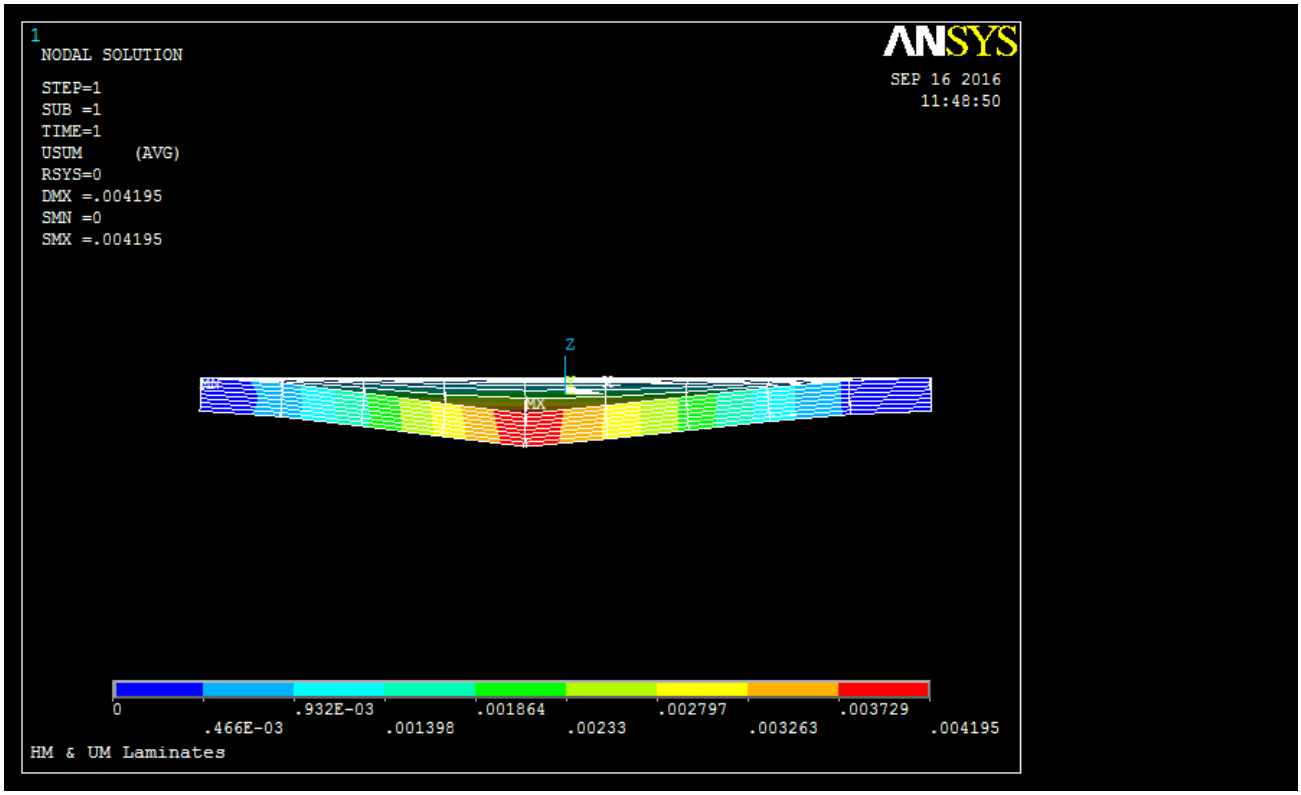

Figure 26. Deflection of HM & UM [(+/-45/0/90)s]n Laminate Design.

(b)

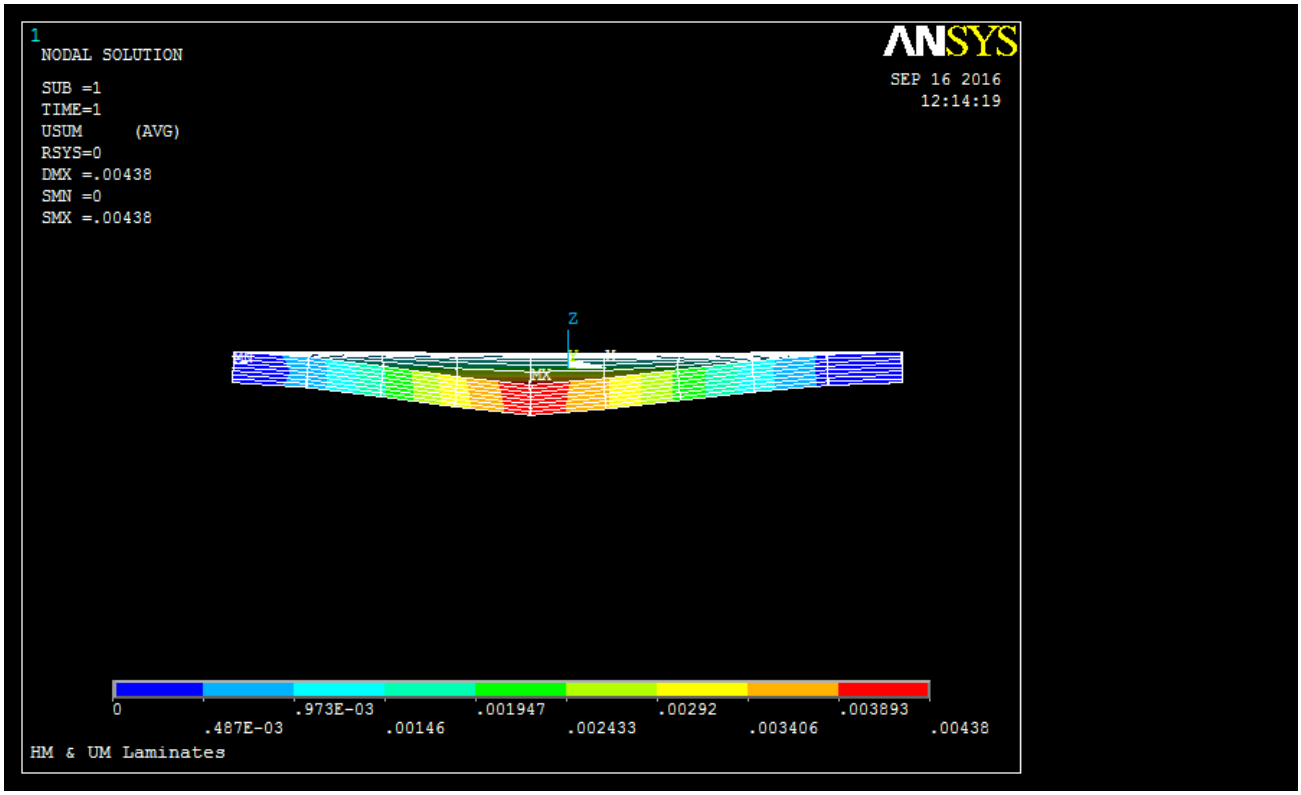

Figure 27. Deflection of HM & UM [(+/-45)s]n Laminate Design.

iii. (a)

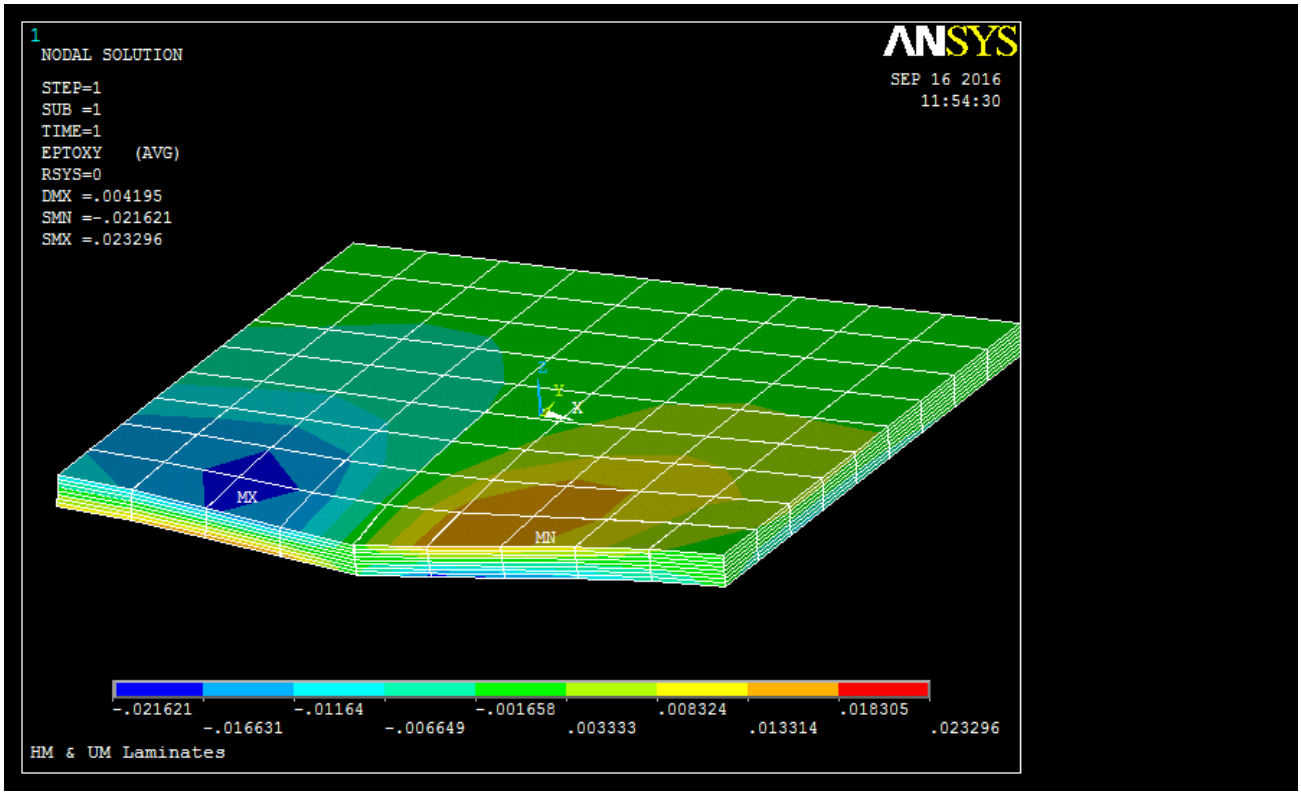

Figure 28. XY Shear Total Mechanical Strain of HM & UM [(+/-45/0/90)s]n Laminate Design.

(b)

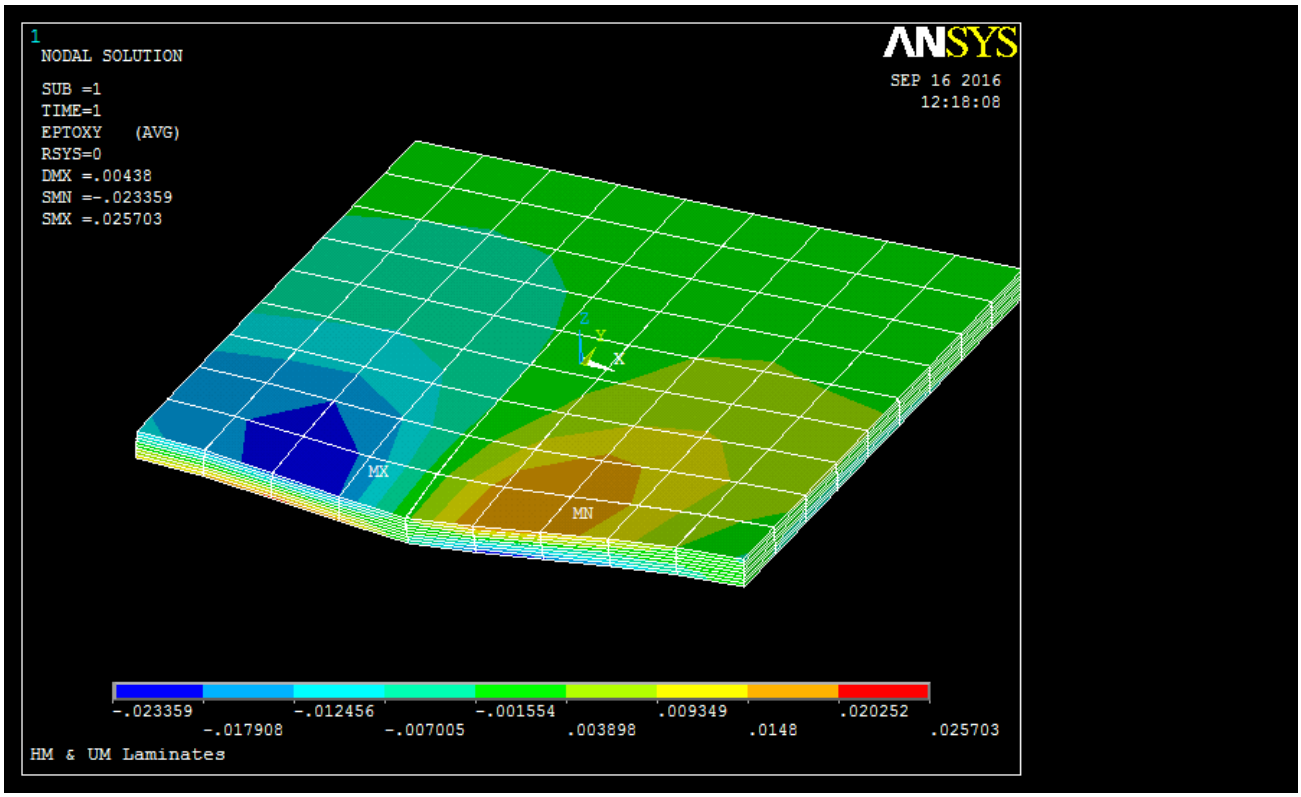

Figure 29. XY Shear Total Mechanical Strain of HM & UM [(+/-45)s]n Laminate Design.

iv. (a)

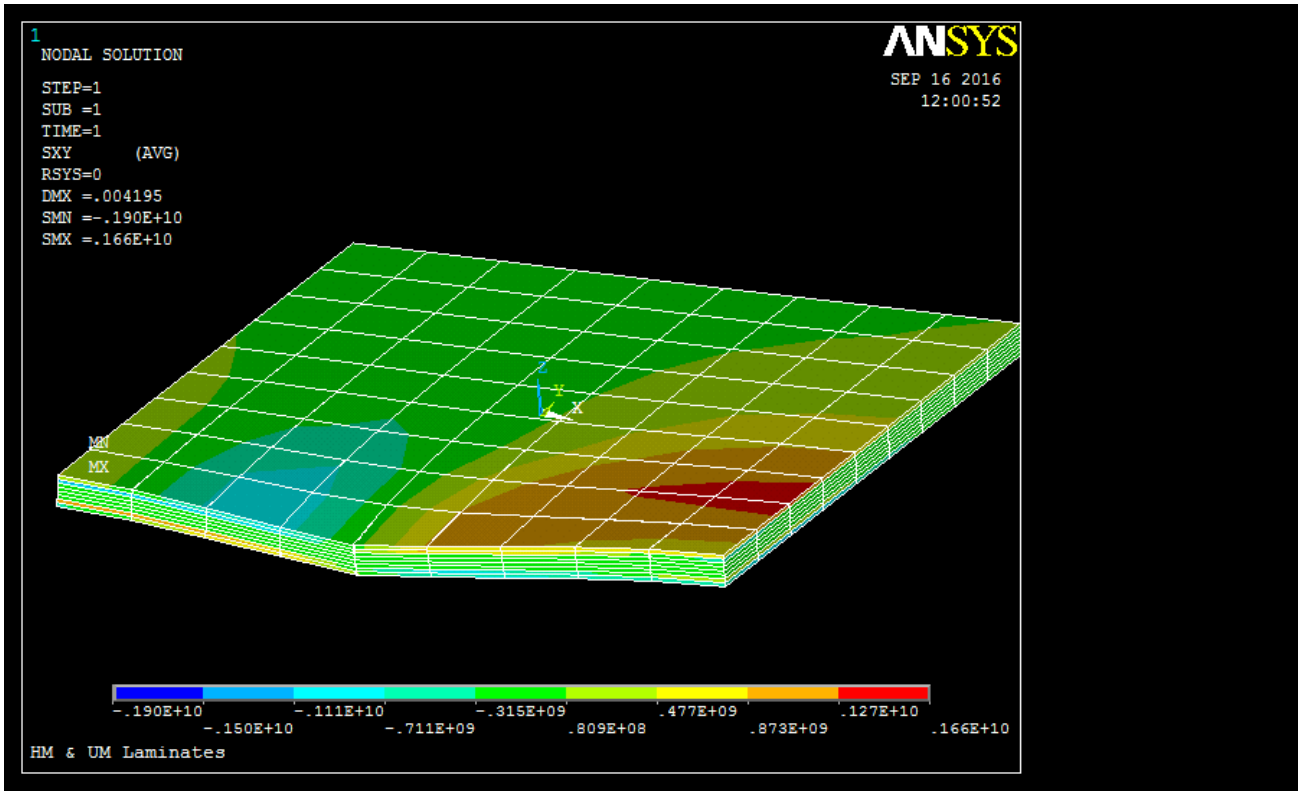

Figure 30. XY Shear Stress of HM & UM [(+/-45/0/90)s]n Laminate Design.

(b)

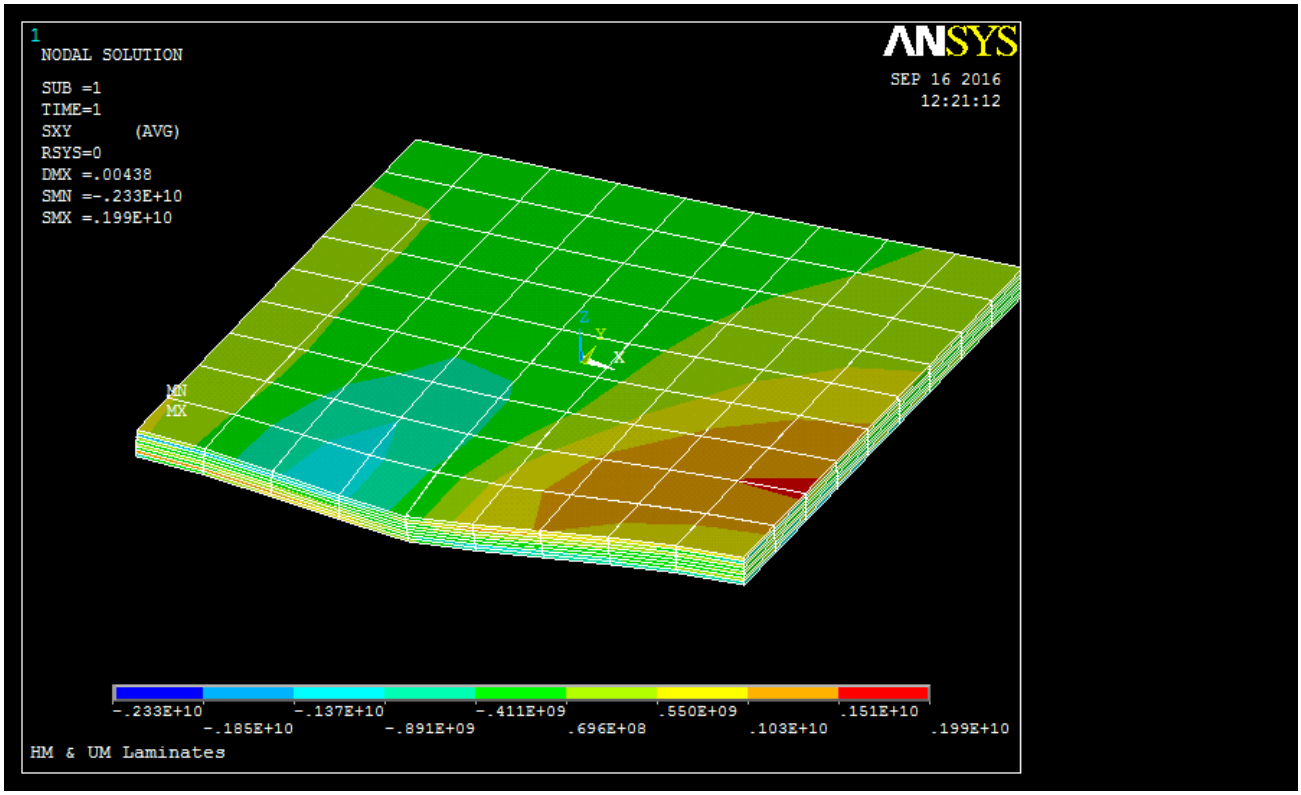

Figure 31. XY Shear Stress of HM & UM [(+/-45)s]n Laminate Design.

v. (a)

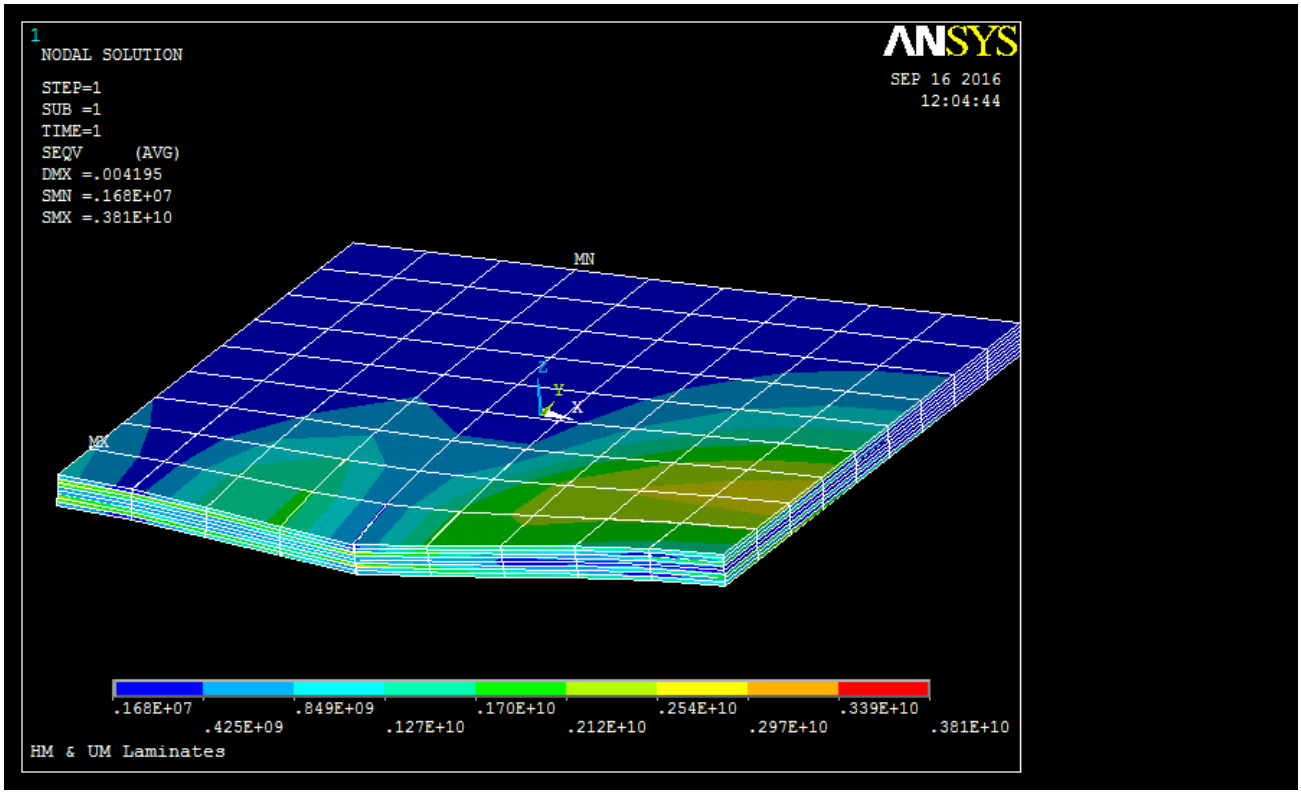

Figure 32. Von Mises Stress of HM & UM [(+/-45/0/90)s]n Laminate Design.

(b)

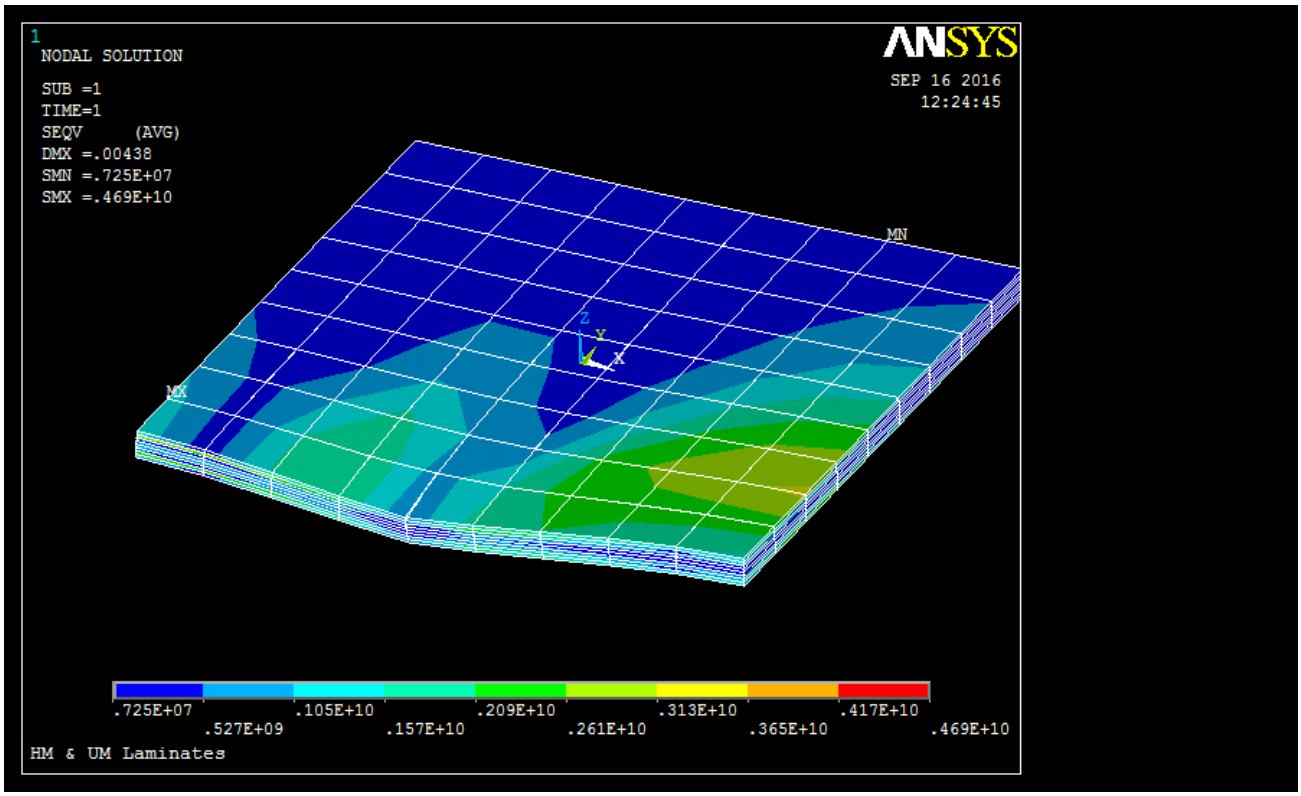

Figure 33. Von Mises Stress of HM & UM [(+/-45)s]n Laminate Design

Table 8. Results for LM Graphite_Epoxy and HM Graphite_Epoxy Laminates Design

S/N	Laminate Analysis	[(+/-45/0/90)s]	[(+/-45)s]
1.	Deflection (m)	0.004869	0.005238
2.	Maximum XY Shear Total Mechanical Strain (m)	0.031911	0.034123
3.	Maximum XY Shear Stress (N/m^2)	0.148E+10	0.164E+10
4.	Maximum Von Mises Stress (N/m^2)	0.362E+10	0.440E+10

Table 9. Results for LM Graphite_Epoxy and UM Graphite_Epoxy Laminates Design

S/N	Laminate Analysis	[(+/-45/0/90)s]	[(+/-45)s]
1.	Deflection (m)	0.004586	0.004941
2.	Maximum XY Shear Total Mechanical Strain (m)	0.030583	0.032305
3.	Maximum XY Shear Stress (N/m^2)	0.160E+10	0.175E+10
4.	Maximum Von Mises Stress (N/m^2)	0.403E+10	0.499E+10

Table 10. Results for HM Graphite_Epoxy and UM Graphite_Epoxy Laminates Design

S/N	Laminate Analysis	[(+/-45/0/90)s]	[(+/-45)s]
1.	Deflection (m)	0.004195	0.00438
2.	Maximum XY Shear Total Mechanical Strain (m)	0.023296	0.025703
3.	Maximum XY Shear Stress (N/m^2)	0.166E+10	0.199E+10
4.	Maximum Von Mises Stress (N/m^2)	0.381E+10	0.469E+10

5.3. Tabulated Summary Results

The various summary results using ANSYS 14.0 mechanical APDL are reflected in Table 8 through Table 10.

The deflections, interlaminar strains (out-of-plane), in-plane shear strengths and Von Misses failure stresses of the three unidirectional graphite-epoxy laminated composite designs (LM and HM, LM and UM, and HM and UM) have successfully been characterized using the finite element method. The influences of deformation rate at failure on the shear strengths and failure mode can be visualized from the displayed graphical images on a macroscopic and a microscopic point of view. The results in Table 8 through Table 10 reveal that;

i. The highest value of maximum interlaminar strain of 0.034123m prior delamination was obtained from design LM and HM with [(+/-45)s] stacking sequence.
ii. The least maximum compressive deformation of 0.004195m was obtained from design HM and UM laminates with [(+/-45/0/90)s] stacking sequence due to its high stiffness property.
iii. The highest value of maximum in-plane shear stress of 0.199×10^{10} N/m^2 is obtained from design HM and UM with [(+/-45)s] stacking sequence.
iv. The highest value of maximum Von-Mises failure stress of 0.499×10^{10} N/m^2 was obtained from design LM and UM with [(+/-45)s] stacking sequence.

6. Conclusion and Recommendations

6.1. Conclusion

The use of Autodesk Simulation Composite Design and ANSYS 14 Mechanical APDL software provided a very close approximation to actual manufacturing process defined within simulation environments. Wing skin laminates design was carried out with the definition of materials or fabrics, orientation of the fibers, determination of ply thickness and laminates stacking sequence. The solid model was then created with the loads and boundary conditions specified. Standard results such as deformations and stresses were therefore displayed on graphical windows.

Autodesk Simulation Composite Design software was used to determine the feasibility of the laminated graphite-epoxy wing skin designs (LM and HM, LM and UM and HM and UM) with their proposed stacking sequences of [(+/-45/0/90)s] and [(+/-45)s], the results revealed that the approximate values of bending, stability and vibration of the various designs were realistic and suitable for further finite element analysis. ANSYS 14 Mechanical APDL which is FEA software provided more accurate analysis and results since solid models of both laminates skin and spar could be meshed via finite element method.

The results obtained from all the three designs of graphite-epoxy proposed for wing skin are relatively close and way beyond the applied shear stress during analysis. As evident in the evaluation of the mechanical properties of the wing skin, stacking sequences of [(+/45/0/90)s] and [(+/-45)s] have marked effect on the mechanical properties of the various designs. When a specimen design is placed under load the fibers tend to rotate in such a way as to align themselves with the loading direction. This movement of fibers gives rise to shear between fibers in the same ply (intra laminar shear) and shear between plies of different orientations (interlaminar shear). Delamination of plies induced by shear stress will occur least in HM and UM with [(+/-45)s] stacking sequence design with maximum shear stress output of 0.199×10^{10} N/m^2. For failure

prediction, employing the Von Mises failure criteria showed that LM and UM with [(+/-45)s] design has the best property prior to failure occurring at 0.499×10^{10} N/m^2. Design HM and UM with [(+/-45/0/90)s] stacking sequence demonstrated least compressive deformation of 0.004195m.

6.2. Recommendation

i. Further research recommendation will be to investigate using computational technique to study the mechanical behaviour of a complete wing structure whose components are now integrated as a single unit made of same graphite-epoxy.
ii. Comparison of the result obtained with that of the skin produced from aluminium materials.

References

[1] Airbus, "*A380 The best solution for 21st century growth*". [Online]. http://www.airbus.com/aircraftfamilies/passengeraircraft/a380family/. Retrieved November 21, 2015.

[2] Akindapo J.O., Johnson-Anamemena N., and Garba D.K., (2017); "*Graphite-epoxy Composite Design for Aircraft Wing Spar Using Computational Techniques – Part I*", American Journal of Mechanical Engineering, Vol. 5, No. 4, 117-127.

[3] ANSYS, Inc., (2013); "*ANSYS Mechanical APDL Structural Analysis Guide*," vol. Release 15, pp. 461-468.

[4] Axel F., (2008); "*Airbus A380:Solutions to the Aerodynamic Challenges of Designing the World's Largest Passenger Aircraft*," in Royal Aeronautical Society, Hamburg Branch / DGLR / VDI / HAW, Hamburg, pp. 9-10.

[5] Carl Zweben. Wiley Online Library (COMPOSITE MATERIALS). [Online]. http://onlinelibrary.wiley.com/doi/10.1002/9781118985960.meh110/pdf. Retrieved September 20, 2016.

[6] James A., Craig C., Phil Y., Ryan L., and James L., (2010); "Airframe Wingbox Preliminary Design and Weight Prediction". Hampton, Virginia, USA: Society of Allied Weight Engineers, (SAWE).

[7] Dan Doherty, "*Toolbox, Analytical Modeling of Aircraft Wing Loads Using MATLAB and Symbolic Math*". [Online]. https://www.mathworks.com/company/newsletters/articles/analytical-modeling-of-aircraft-wing-loads-using-matlab-and-symbolic-math-toolbox.html. Retrieved May 18, 2016.

[8] Department of Defense Handbook, (2002); "*Polymer Matrix Composites Materials Usage, Design and Analysis*," vol. 3, pp. 2-1 to 2-15.

[9] Fabrice B., (2015); "*Global Market Forecast (Flying by Numbers 2015 2034),*" "*We Are Focused on our Long-Term Future More than Ever Before*," no. 2, pp. 032-033.

[10] Martin H., (2003); "*Composite Aircraft Design*", 5th ed., Ed. Monterey, California: Martin Hollmann.

[11] Shabeer K.P. and Murtaza M. A., (2013); "*Optimization of Aircraft Wing with Composite Material*," International Journal of Innovative Research in Science, Engineering and Technology, vol. 2, no. 6, pp. 2471-2477.

[12] Sudhir R. K. and Sujatha Y., (2015); "*Design and Analysis of Aircraft Wing*," International Journal and Magazine of Engineering, Technolog, Management and Research , vol. 2, no. 9, pp. 1480-1487.

[13] Suresh K. J., Vijaya K. R. K., and Sidda R. B., (2013); "*Prediction of Deflection and Stresses of Laminated Composite Plate with an Artificial Neural Network Aid*," International Journal of Applied Science and Engineering, vol. 11, no. 4, pp. 393-413.

[14] Wahab U. M., Riaz A., Iqbal R. and Hassan N. K., [Online]. http://www.wseas.us/e-ibrary/conferences/2013/Brasov/ICAPS/ICAPS-01.pdf. Retrieved July 5, 2016.

[15] William D. C. Jr. and David G. R., (2010); "*Materials Science and Engineering an Introduction"*, 8th ed., William D. Callister Jr. and David G. Rethwisch, Ed. United States of America: Wiley & Sons, Inc., 111 River Street, Hoboken.